Determination of the fraction of J/ψ produced via radiative decays of χ_c

O.Igonkina
ITEP, Moscow

February 6, 2002

Abstract

The analysis of the year 2000 data taken with use of Carbon and Titanium targets is presented. The triggered data of $J/\psi \to \mu^+\mu^-$, $J/\psi \to e^+e^-$ are used to reconstruct the radiative decays $\chi_{c1} \to J/\psi\gamma$, $\chi_{c2} \to J/\psi\gamma$. The signal of the χ_{c1} and χ_{c2} states is observed both in muon and electron samples. The ratio $R_{\chi_c} = \sigma(\chi_c)Br(\chi_c \to J/\psi\gamma)/\sigma(J/\psi)_{tot}$ is estimated to be 0.36 ± 0.07 for Carbon and 0.31 ± 0.11 for Titanium.

Contents

1 Introduction. Definition of R_{χ_c} .

The charmonium system and its production in hadronic collisions has recently attracted considerable attention from both theoretical and experimental sides for two different reasons, namely, understanding of the production mechanism and the influence of the nucleus on production cross section.

Schematically, the production mechanism consists of the creation of a $c\bar{c}$ pair in the interaction of gluons and/or quarks followed by the formation of a charmonium state from an unbound pair. The first step can be calculated in pQCD. However, the process of formation of the bound state is not understood. Three different models compete to describe the production of heavy quarkonium: the Colour Singlet Model (*CSM*)[1], non relativistic QCD (*NRQCD*)[2], and the Colour Evaporation Model (*CEM*)[3].

The measurement of the relative production ratio of the J/ψ and χ_c [1] states in hadronic collisions is a sensitive test of the production mechanism which can be done relatively easy at HERA-B . The leptonic decays of the J/ψ provide an excellent signature for triggering. The well known radiative decays of $\chi_c \to J/\psi\gamma$ provide a base to study the production cross section of the χ_c mesons, the characteristic value being

$$R_{\chi_c} \equiv \frac{\sigma(\chi_{c1})Br(\chi_{c1} \to J/\psi\gamma) + \sigma(\chi_{c2})Br(\chi_{c2} \to J/\psi\gamma)}{\sigma(J/\psi)_{tot}} \quad (1)$$

The theoretical predictions on this ratio diverge. The CSM model predicts $R_{\chi_c}^{CSM} = 0.7$, NRQCD gives $R_{\chi_c}^{NRQCD} = 0.3$ for $p-A$ interactions. The CEM does not give an absolute number but requires the ratio to be independent of beam and target material and of the c.m.s energy $\sqrt{s}$. $\pi - A$ and $p - A$ data yield $R_{\chi_c}^{CEM} = 0.4$ [4]. The existing measurements of R_{χ_c} are summarised in table 1. These measurements together with the studies of the absolute and differential cross section of J/ψ [5] favour NRQCD model but not rule out completely CSM and CEM. The J/ψ and $\psi(2S)$ polarisation[6] data do not support all these models but do not exclude them either. More experimental data are required to distinguish between the models.

The production rate is also influenced by the presence of the nucleus. There are several models which try to take into account changes of the initial parton density functions and/or absorption of the produced $c\bar{c}$ pair (see [8] for a review). It has been suggested that the production rate of charmonium can be expressed by the function

$$\sigma_{pA} = \sigma_{pN} \cdot A^{\alpha}, \quad (2)$$

[1] Here and further the χ_c stands for the combination of the χ_{c1} and χ_{c2} states. We will also indicate J/ψ originating from χ_{c1} or χ_{c2} by *non-direct* J/ψ .

Exp.	E673	ISR	E705	E771	CDF
Target	Be	p	Li	Si	$\bar{\text{p}}$
$\sqrt{s}[GeV]$	$\tilde{2}0$	52,63	23.7	38.8	1800
$N(J/\psi)$	157		6090	11660	32640
$N(\chi_c)$	11.8		250	66	1230
ε_γ [%]	16		16	0.825	13.5
$\sigma_M(\chi_c)$ $[\frac{MeV}{c^2}]$	15		30	5.2	50-55
$R_{\chi_c}[\%]$	47±23	47 ± 8	30±4	69 ± 8^1	29.7 ± 5.9
$\sigma(\chi_{c1})/\sigma(\chi_{c2})$	0.24 ± 0.28	-	-	0.53 ± 0.21	1.12

Table 1: The world measurements of the χ_c production in the pp, $p\bar{p}$, $p-A$ collisions. The number of observed J/ψ $(N(J/\psi))$ and χ_c $(N(\chi_c))$ events are shown together with the efficiency of photon reconstruction ε_γ and the mass resolution of the χ_c signal $(\sigma_M(\chi_c))$. The measured fraction of J/ψ produced via χ_c R_{χ_c} is presented as well as a cross section ratio of the χ_{c1} to χ_{c2}. ^{1}) The E771 R_{χ_c} value is deduced from the published cross sections $\sigma(\chi_{c1})$, $\sigma(\chi_{c2})$ and $\sigma(J/\psi)$. The references could be found in [7].

where σ_{pN} is the production cross section of the given state in proton-nucleon interactions and A is the atomic mass of the nucleus. The parameter α represents the combination of different nuclear effects. As was shown in [9] χ_c production is expected to be more sensitive to the nuclear effects than J/ψ production. However, the mean value of the parameter α is around 0.92 for both kind of mesons, and the variation of α does not exceed 0.02 [9]. This translates into an expected increase of the value of R_{χ_c} of 0–5% for Carbon and 0–8% for Titanium, respectively, compared to the proton data.

At present, nuclear suppression of the production of the the different charmonium states is measured only for J/ψ and ψ', and only in the positive x_F region[2].

A measurement of R_{χ_c} with a relative precision of better than 5% over a large kinematic region would give insight into nuclear effects. Even a measurement with a relative precision of better than 20% will significantly improve our knowledge on the relative production ratio of J/ψ and χ_c in proton-nucleus interactions, and will help us to understand the production mechanism.

[2] x_F is the longitudinal momentum fraction $x_F = p_z/p_z^{max}$ in the c.m. system.

2 Outline of the analysis

We present here an analysis of χ_c production based on HERA-B data of the year 2000. The analysis is based on the radiative decay of $\chi_c \to J/\psi\gamma$, based on the $J/\psi \to \mu^+\mu^-, e^+e^-$ channels. The χ_c is observed as a signal in the distribution of the invariant mass difference $\Delta M = M(l^+l^-\gamma) - M(l^+l^-)$. R_{χ_c} has been extracted using the equation:

$$R_{\chi_c} = \frac{N_{\chi_c}}{N_{J/\psi}\varepsilon_\gamma}, \tag{3}$$

where N_{χ_c} and $N_{J/\psi}$ are the numbers of reconstructed χ_c and J/ψ , respectively, and ε_γ represents the photon reconstruction efficiency. We assume the trigger and reconstruction efficiencies for direct J/ψ and χ_c events to be equal.

The outline of the note repeats the selection chain of the χ_c events. First the trigger of J/ψ and its influence on event characteristics are discussed. After the description of the data samples the reconstruction of the J/ψ leptonic decays and the measurement of $N_{J/\psi}$ are described in sec.6. Section 7 is dedicated to the cuts on multiplicity. The photon is reconstructed as a cluster in the ECAL subsystem. The selection of the photon candidates and the estimation of the photon reconstruction efficiency ε_γ is presented in sec.8. The measurement of the N_{χ_c} is described in sec.9. The study of the systematic uncertainties is reported in sec.10. At the end the R_{χ_c} value is calculated and compared with other measurements and theoretical predictions (see sec.11).

Before the attention will be absorbed by details of the analysis we would like to explain the choice of the ΔM distribution and the procedure of the cuts optimisation.

2.1 Mass $M(l^+l^-\gamma)$ or Mass Difference $\Delta M = M(l^+l^-\gamma) - M(l^+l^-)$.

Taking into account that the vertex of the J/ψ production is identical to the vertex of the J/ψ decay the invariant mass of the χ_c reconstructed in the channel $J/\psi\gamma$ is:

$$M_{\chi_c} = \sqrt{M^2_{J/\psi} + 2E_\gamma E_{J/\psi} - 2\vec{p}_\gamma \vec{p}_{J/\psi}} \tag{4}$$

Neglecting the correlation between $M_{J/\psi}$ and $\vec{p}_{J/\psi}$ and the cluster energy resolution the error in determination of M_{χ_c} will be related with error on $M_{J/\psi}$ as:

$$\delta M_{\chi_c} = \frac{M_{J/\psi}}{M_{\chi_c}} \delta M_{J/\psi} = 0.877 \cdot \delta M_{J/\psi} \tag{5}$$

Or in other words the width of the χ_c will be of the same order as width of J/ψ . From other side the mass difference of the states $\Delta M = M(J/\psi\gamma) - M(J/\psi)$ should be significantly narrower:

$$\delta(M_{\chi_c} - M_{J/\psi}) = (\frac{M_{J/\psi}}{M_{\chi_c}} - 1)\delta M_{J/\psi} = -0.123 \cdot \delta M_{J/\psi} \tag{6}$$

Therefore the widths of 2 distributions will be related as

$$\frac{\delta M_{\chi_c}}{\delta(M_{\chi_c} - M_{J/\psi})} = \frac{M_{J/\psi}}{M_{J/\psi} - M_{\chi_c}} \approx 7 \tag{7}$$

The level of the background in the equal mass interval (e.g. 10MeV/c^2) is twice higher for the ΔM with respect to the mass distribution. However, in the interval of ± 2 standard deviations the background in the ΔM spectrum will be 3.5 times smaller. Even taking into account that the contribution of the photon energy resolution will decrease this ratio, the signal will be more pronounced in ΔM distribution.

Fig.1 shows a typical spectrum for the mass difference ΔM. The enhancement at ΔM = 0.43 GeV/c^2 corresponds to the sum of the χ_{c1} and χ_{c2} states. The background is due to other clusters present in the event.

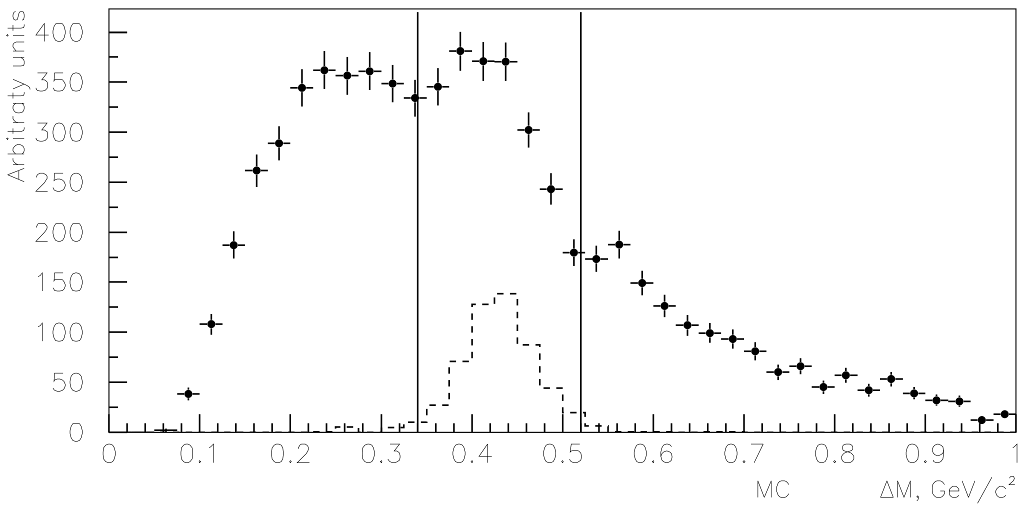

Figure 1: ΔM distribution obtained on MC sample with χ_c states. The curve below shows true combinations of J/ψ and photon from χ_c decays. The lines indicate the interval used for optimisation of cuts.

2.2 Optimisation of cuts

Optimisation of the selection criteria for the lepton tracks and the J/ψ is achieved by maximazing the value

$$\eta = \frac{N_{\chi_c}}{\sigma(N_{\chi_c})} = \frac{S}{\sqrt{D}} \tag{8}$$

in the ΔM distribution, where $\sigma(N_{\chi_c})$ is the error on the estimate of the number of χ_c mesons. The signal $S = N_{\chi_c}$ is considered to be proportional to $N_{J/\psi} \cdot \varepsilon_\gamma$, where $N_{J/\psi}$ is estimated on data. The value D is taken as the number of events in the interval of width $\pm 2\sigma_M$ around the position of the χ_c in the ΔM distribution as indicated in fig.1.

Since the cuts might be correlated, the optimal value of any cut was checked for stability for different sets of other cuts applied.

3 Detector.

HERA-B is a fixed target experiment located at the HERA proton storage ring at DESY (Hamburg). The energy of the proton beam is 920 GeV which gives the energy in the c.m. frame $\sqrt{s} = 41.6$ GeV. The target consists of 8 wires of different materials, two of which (C and Ti) were used during the period of data taking analysed. During operation, the wires are inserted into the halo of the beam. The good resolution of reconstructed vertices allows to separate the primary interactions on the different wires [10]. The interaction rate varied between 5 and 10 MHz. At 5 MHz interaction rate, each event contains on average 0.5 primary interactions distributed accordingly to Poissonian statistics.

A schematic layout of the detector is presented in Fig.2. The tracker consists of 3 parts : a silicon vertex detector, micro strip gas chambers (the inner tracker) and honeycomb drift chambers (the outer tracker). The 2.2 Tm magnet is positioned in the middle of the spectrometer and gives a 0.64 GeV/c transverse momentum kick to charged particles. Particle identification devices include a ring imaging Cherenkov counter (*RICH*), an electromagnetic calorimeter, and a muon system. A detailed description of the detector can be found elsewhere[11].

The detector covers a large pseudo-rapidity interval $\eta \in [2, 5]$, corresponding to an interval $x_F \in [-0.4, 0.3]$ for J/ψ. During the year 2000, the inner tracker was not in use restricting the acceptance to $x_F \in [-0.4, 0.1]$.

The detector allows complete event reconstruction including the neutral particles such as γ and π^0. The photon efficiency is around 30% which is significantly higher than in most of the experiments cited in tab.1.

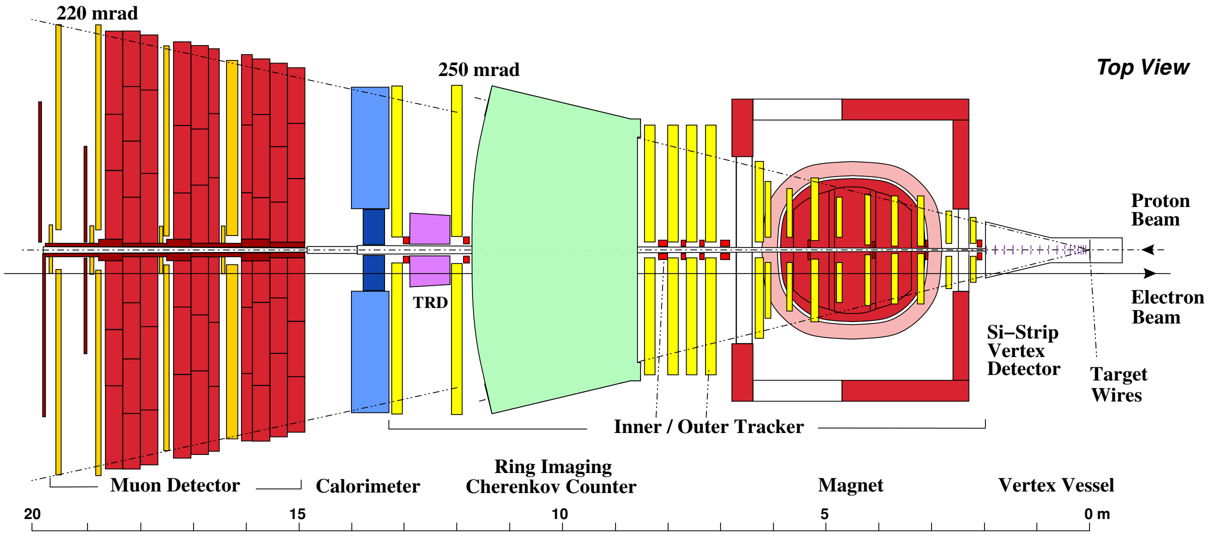

Figure 2: The HERA-B detector.

The cross section for J/ψ production is small compared to the inelastic cross section: $\sigma_{J/\psi}/\sigma_{in} = 3 \cdot 10^{-5}$.

4 Trigger.

Among other triggers HERA-B uses a J/ψ trigger which selects lepton pairs (e^+e^- or $\mu^+\mu^-$) with a high invariant mass. With trigger *μ-SLICER* tracks with hits in at least three muon super-layers are classified as muon tracks. The transverse momentum of muons is required to be larger than 0.7 GeV/c. For the electron trigger *e-SLICER* the transverse energy deposited in the calorimeter by each candidate is required to be greater than 1 GeV/c.

Table 2 shows an trigger efficiency for different J/ψ events. The efficiency is in the range of 1.4-2%. The calculation is done for each J/ψ production model. The efficiencies of the trigger affects the R_{χ_c} ratio as:

$$R_{\chi_c} = \frac{\sigma(\chi_c)Br(\chi_c \to J/\psi\gamma)}{\sigma(J/\psi_{dir}) + \sigma(\chi_c)Br(\chi_c \to J/\psi\gamma)} = \frac{N^{trig}_{\chi_c}/\varepsilon_{\chi_c}}{N^{trig}_{J/\psi}/\varepsilon_{all}} \tag{9}$$

In the cases of NRQCD and CSM, the ratio of the trigger efficiency for non-direct and all J/ψ $R_\varepsilon = \varepsilon^{\chi_c}/\varepsilon^{all}$ is close to 1. In the case of CEM, the kinematic spectra of direct and non-direct J/ψ are the same resulting in $R_\varepsilon = 1$ as well.

Model	E789	NRQCD	CSM
		e-SLICER, C	
All J/ψ	$1.94 \pm 0.03\%$	$1.82 \pm 0.03\%$	$1.89 \pm 0.03\%$
Direct J/ψ	-	$1.78 \pm 0.03\%$	$1.91 \pm 0.04\%$
Non-direct J/ψ	-	$1.93 \pm 0.05\%$	$1.95 \pm 0.04\%$
J/ψ from χ_{c1}	-	$1.85 \pm 0.06\%$	$1.77 \pm 0.09\%$
J/ψ from χ_{c2}	-	$1.99 \pm 0.07\%$	$1.87 \pm 0.04\%$
		e-SLICER, Ti	
All J/ψ	$1.95 \pm 0.05\%$	$1.87 \pm 0.04\%$	$1.90 \pm 0.05\%$
Direct J/ψ	-	$1.78 \pm 0.05\%$	$1.91 \pm 0.07\%$
Non-direct J/ψ	-	$2.10 \pm 0.09\%$	$1.98 \pm 0.06\%$
J/ψ from χ_{c1}	-	$2.17 \pm 0.11\%$	$2.02 \pm 0.16\%$
J/ψ from χ_{c2}	-	$1.96 \pm 0.12\%$	$1.84 \pm 0.06\%$
		μ-SLICER, C	
All J/ψ	$1.35 \pm 0.02\%$	$1.42 \pm 0.02\%$	$1.39 \pm 0.02\%$
Direct J/ψ	-	$1.39 \pm 0.02\%$	$1.41 \pm 0.03\%$
Non-direct J/ψ	-	$1.50 \pm 0.03\%$	$1.43 \pm 0.02\%$
J/ψ from χ_{c1}	-	$1.55 \pm 0.04\%$	$1.44 \pm 0.06\%$
J/ψ from χ_{c2}	-	$1.41 \pm 0.05\%$	$1.35 \pm 0.02\%$
		μ-SLICER, Ti	
All J/ψ	$1.33 \pm 0.03\%$	$1.40 \pm 0.03\%$	$1.36 \pm 0.03\%$
Direct J/ψ	-	$1.39 \pm 0.03\%$	$1.41 \pm 0.04\%$
Non-direct J/ψ	-	$1.45 \pm 0.05\%$	$1.38 \pm 0.04\%$
J/ψ from χ_{c1}	-	$1.49 \pm 0.07\%$	$1.38 \pm 0.09\%$
J/ψ from χ_{c2}	-	$1.38 \pm 0.07\%$	$1.32 \pm 0.04\%$

Table 2: The efficiency of the different triggers for J/ψ of the different origin. The estimations is done for 3 models. The errors shown reflect the size of the MC statistics . The accuracy of the NRQCD and CSM implementation brings extra relative uncertainty of 0.05%.

Since the J/ψ and the photon from the radiative χ_c decay have very small momenta in the χ_c rest frame, they have almost parallel momenta in the lab system. Since the trigger selects J/ψ s within a certain kinematic region (see fig.3), the acceptance for the photon (p_T^γ, x_F^γ) is affected as well. Fig.4 shows the dependence of the photon energy on the $x_F(J/\psi)$. One sees correlation between fast J/ψ and energetic photons. Fig.5 presents the energy, the polar angle and the transverse energy of the photon before and after the trigger. Obviously, the electron trigger selects more energetic photons which are closer to the beam than the muon trigger.

5 Data used for Analysis

Sample	Time Period	Runs	Target	Trigger	Channel	N J/ψ
A	8.06-24.07	15800-16669	C	e-SLICER	e^+e^-	1445 ± 93
B	25.07-17.08	16670-17100	C, Ti	e-SLICER	e^+e^-	1259 ± 82
C	1.07-24.07	16000-16669	C	μ-SLICER	$\mu^+\mu^-$	1559 ± 48
D	25.07-17.08	16670-17100	C, Ti	μ-SLICER	$\mu^+\mu^-$	1897 ± 59

Table 3: The data periods used in the analysis. The wires used are C - carbon inner 2 and Ti - titanium below 1. The trigger type SLICER is also known as SLICER/REFIT. $N(J/\psi)$ means the number of the reconstructed J/ψ with the lepton identification but without the additional restriction for χ_c analysis (see below). The number of $J/\psi \to e^+e^-$ is estimated according to eq.13.

Collection	Channel	Target Material	N J/ψ	sample used
e-C	e^+e^-	C	1981 ± 104	A, half B
e-Ti	e^+e^-	Ti	725 ± 60	half B
μ-C	$\mu^+\mu^-$	C	2412 ± 60	C, half D
μ-Ti	$\mu^+\mu^-$	Ti	1070 ± 41	half D

Table 4: The subsamples for final analysis.

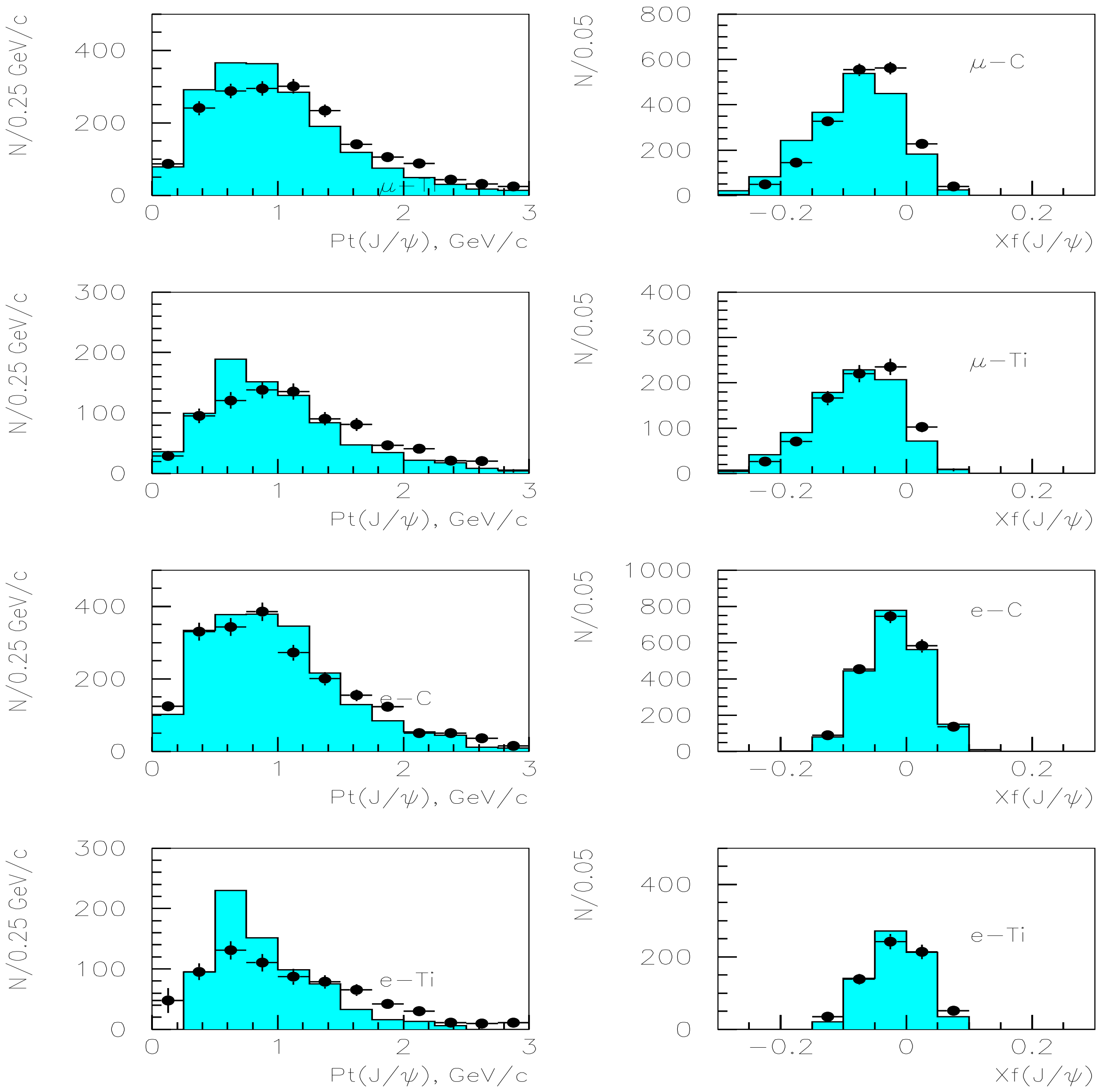

Figure 3: The kinematic spectra of J/ψ for each sample. The points show the number of J/ψ estimated from the di-lepton invariant mass fit. The shaded histograms show the MC spectra of the triggered J/ψ events according to the NRQCD prediction. No correction for nuclear effects is performed. Although the MC spectra are close to the measured ones the usage of NRQCD together with nuclear dependence measured by E866 describes better the p_T spectra. The $x-F$ spectra remain not well described (see [12]).

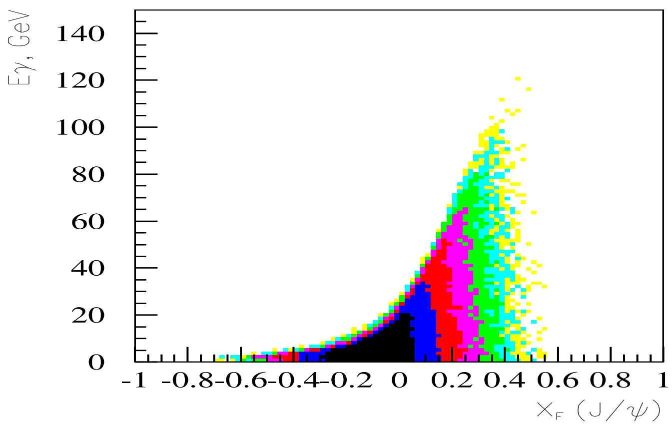

Figure 4: MC: $\chi_c \to J/\psi\gamma$ events. The correlation of the photon energy E_γ and $x_F^{J/\psi}$.

5.1 Data Samples and Data Quality checks.

The analysis is based on data which were collected in summer 2000 in parallel with the commissioning of the detector and the optimisation of the trigger. This implies periods with different trigger and with different target combinations (see tab.3). In the cases when two different targets were used simultaneously, the assignment of the event to the target wire is done on the base of the J/ψ vertex position (see fig.6). The final results are presented separately for the two J/ψ decay channels and the two target materials (see. tab.4).

The following data quality checks were performed for each run:

- **The stability of the average number of the reconstructed hits (N_{hit}) per each sub-detector and the average number of hits (N_{hit}^{track}) associated with tracks.** The first number should be proportional to the number of properly working channels. The difference between the first and the second number reflects the amount of the *hot* channels. If N_{hit} or N_{hit}^{track}/N_{hit} exceeds the average number over the complete period by more than 4 standard deviations the run is rejected (see fig.7). The check was performed for the subsystems SVD, OTR, ECAL and MUON on the basis of the minimum bias events from the same runs. The period 16300-16550 contains some runs with an extreme amount of hits in SVD and ECAL. These runs were removed from the analysis as well. A series of runs around 16900 have a very high occupancy as well, but do not contain triggered events (*minimum bias* runs).

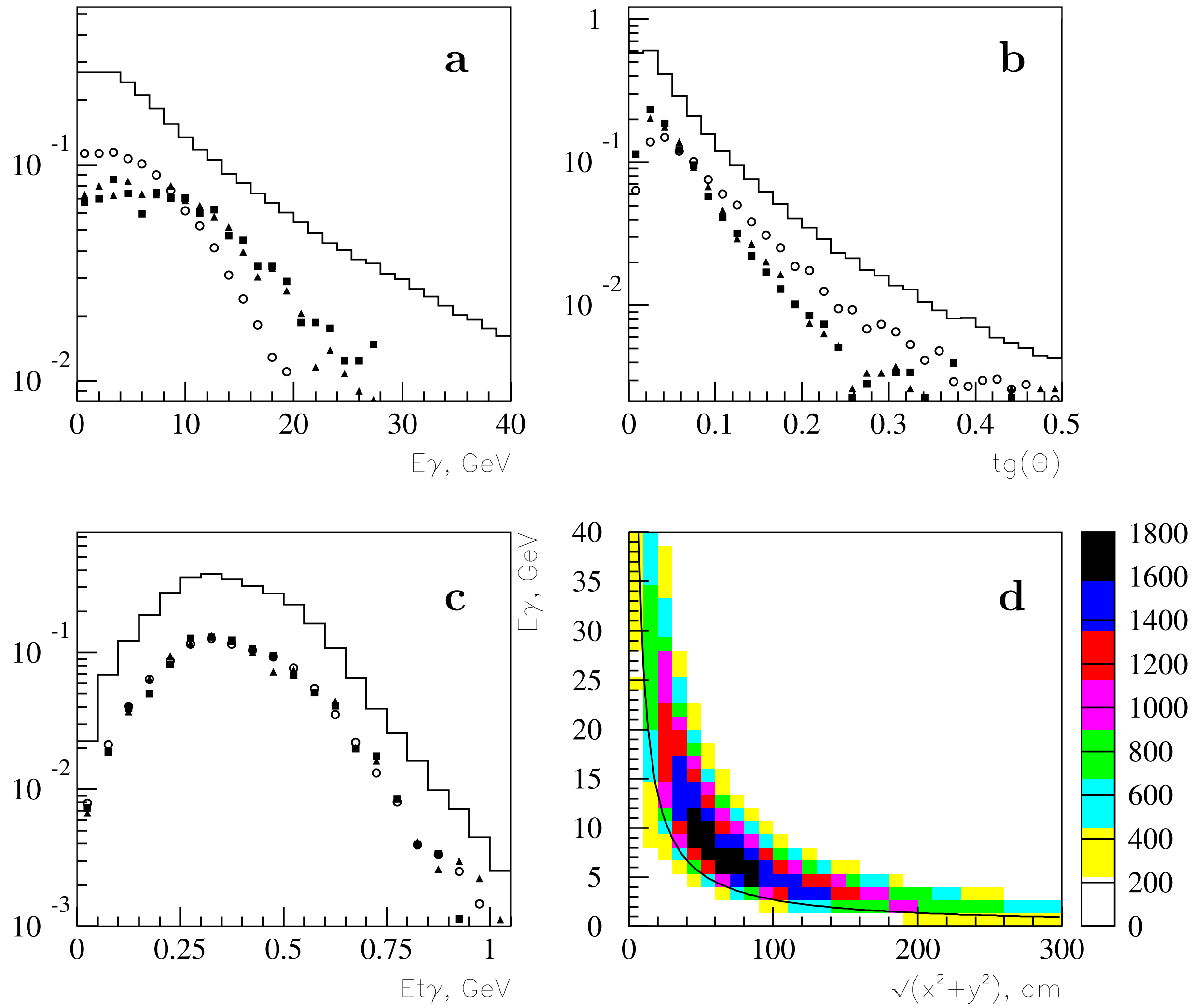

Figure 5: The MC spectra of the photon from χ_c . a) The energy of photon E_γ; b) The angle Θ between direction of the photon and axis z; c) The transverse energy of the photon $E_{T\gamma}$; d) E_γ versus $R = \sqrt{x^2+y^2}$, where x, y are the coordinates of the intersection of photon direction and ECAL surface. On the fig. a-c the histograms shows the distributions before the trigger is applied; squares, triangles and circles corresponds to the events selected by $e - FLT$, e-SLICER, μ-SLICER triggers respectively. The normalisation is arbitrary.

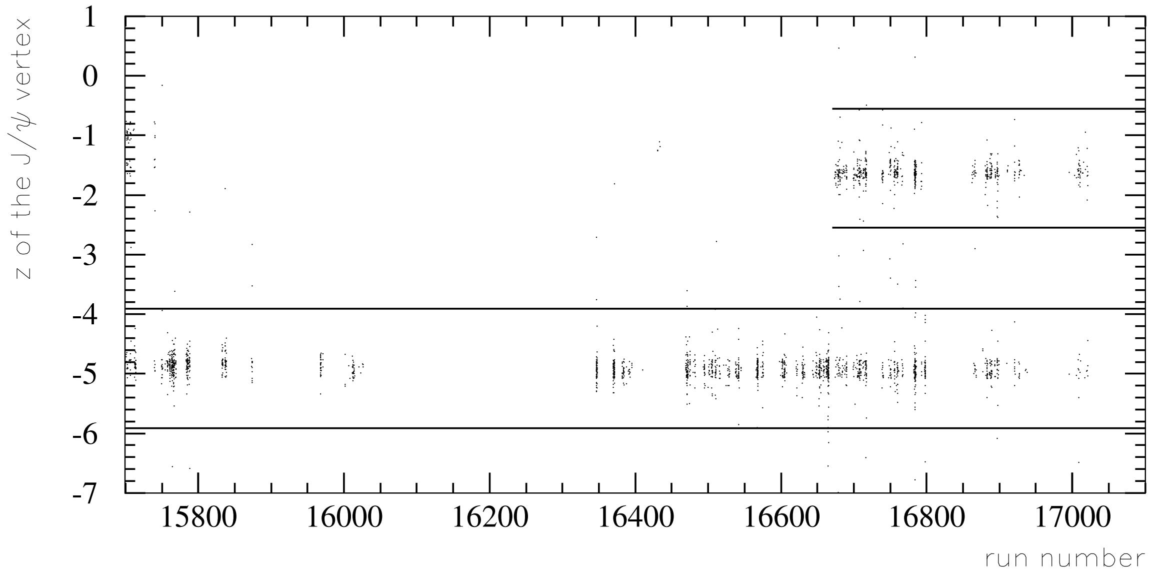

Figure 6: The z coordinate of the J/ψ vertex as function of the run. The line shows the assignment to the target.

- **Interaction out-of-time or out-of-target.** Here one can consider three types of problems :
  - **The presence of the coasting beam.**

    As was shown in [13] the coasting beam was present in runs with operation of the "outer" or "above" wires of the target. The coasting beam causes events which are not synchronised with the proton beam bunch structure, and which therefore have not been registered properly by the detector. When only the "inner-2" or "below-1" wires were used no significant coasting beam was observed.
  - **Unequal beam structure**.

    Since the relative production rates of J/ψ and χ_c does not depend on the intensity of the bunch, the unequal bunch structure is not a problem for this analysis. However, the high occupancy events which are probable during such runs can affect the reconstruction of χ_c and therefore should be treated carefully (see section "Multiplicity").
  - **The interaction of the proton with gas, not with target**.

    The target is associated with the event on the base of the position of the reconstructed J/ψ vertex. It turns out that the J/ψ vertex is practically always on the one of the target [10].

- **The stability of the trigger**. The number of reconstructed J/ψ was checked for each trigger type. The signal to background ratio was constant within errors.
- **The alignment between SVD and ECAL** was checked for each period via the correlation of the linear prolongation of the VDS segment and the position of the ECAL cluster (*bremsstrahlung*). The observed shifts were corrected before the final reconstruction was performed [14].
- **The ECAL calibration coefficients** were found to be constant within 2% [15]. The electronic noise turned out to be a problem for the reconstruction of soft clusters, and a special algorithm of noise suppression was designed to compensate the effect [16].

5.2 Monte Carlo

The simulation of the J/ψ and the inelastic events was done in four steps:

- The generation of J/ψ events was done with PYTHIA[17] while inelastic background was simulated by FRITIOF/ADRIADNE[18]. The kinematic spectra of J/ψ and χ_c were weighted according to the NRQCD predictions[19]. As a cross check, the CSM predictions and the measured spectra of E789 were used for the study of the systematics. No CEM simulation was available for the analysis.

  The ratios of the different charmonium states produced and decayed into J/ψ , as predicted by the different models, are summarised in table 5. E789 published only the differential cross section of J/ψ production integrated over all charmonium states. Model "E789" [20] serves as a benchmark for the standard HERA-B MC. The charmonium ratios used in model "E789" do not have any physical meaning.

Model	direct J/ψ	χ_{c0}	χ_{c1}	χ_{c2}	$\psi(2S)$	R_{χ_c}
NRQCD	67%	0.2%	17%	13%	3%	0.3
CSM	29%	3%	4%	61%	3%	0.65
E789	60%	2%	10%	28%	0%	0.38

Table 5: The production ratios of different charmonium states for the different models used in the simulation. The values includes the branching ratio of decays charmonium to J/ψ [22].

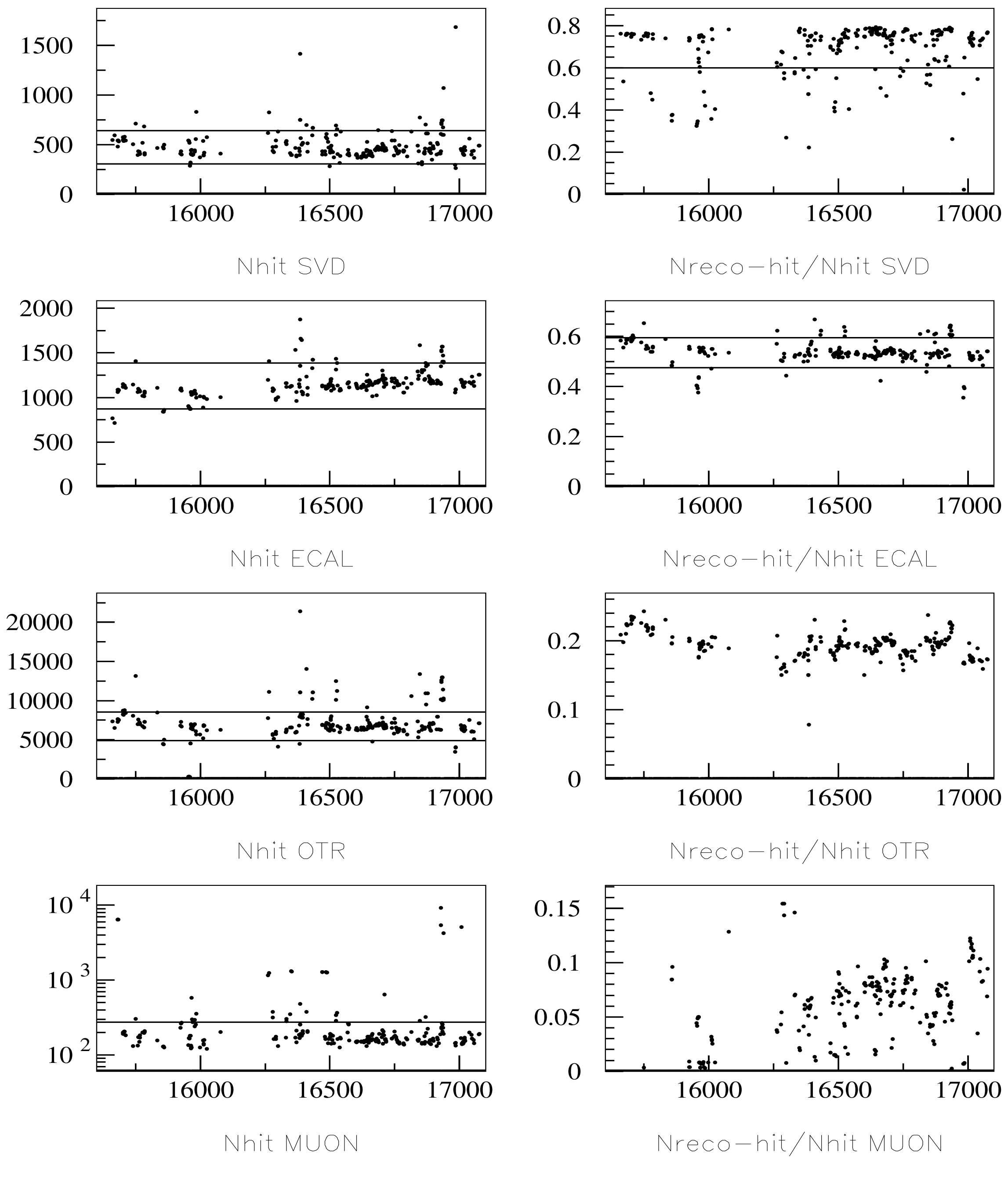

Figure 7: Average number of the reconstructed hits (N_{hit}) per each sub-detector for each run and the average number of hits (N_{hit}^{track}) associated with tracks over N_{hit} for each run.

- The response of the detector was simulated with GEANT[21], using the geometry files 99.813, 99.1014 and 99.1015[23]. No significant difference was found between different geometries. The detector maps and constants were taken from the run 16665. The realistic hit resolution and the position of dead channels were taken into account. Special attention was paid to the simulation of the ECAL response (see below).

  To simulate the realistic number of interactions per event one J/ψ event was mixed with several inelastic events distributed according to Poisson statistics with an average of 0.5. However, the detector occupancy of the MC events is underestimated with respect to real events (see the discussion on multiplicity below).

- The simulated data were given on the input of the trigger chain used during data taking. The reconstruction scheme was identical to the one used for the real data.

The MC statistics used for analysis is summarised in tab.6

Channel	Material of Target	Trigger	Run Masks	$N^0_{J/\psi}$	$N^{trig}_{J/\psi}$
$J/\psi \to ee$	C	e-SLICER	16665	$2.74 \cdot 10^5$	5409
$J/\psi \to ee$	Ti	e-SLICER	16665	$9.4 \cdot 10^4$	1922
$J/\psi \to \mu\mu$	C	μ-SLICER	16665	$5 \cdot 10^5$	9004
$J/\psi \to \mu\mu$	Ti	μ-SLICER	16665	$2 \cdot 10^5$	3005

Table 6: The Monte Carlo samples used in the analysis.

6 Reconstruction of J/ψ .

6.1 Lepton reconstruction.

Reconstruction was performed with ARTE-03-09-r5, using the RTRA2001 chain with KEYBOOK 17. This produced tracks of the SVD-OTR pairs with ECAL cluster or MUON tracks attached. In addition the SVD tracks combinations with energetic ECAL clusters ($E_T > 0.9$ GeV) were considered. The tracks with similar direction and momenta:

$$\begin{cases} \sqrt{\left(\frac{p_{x1}}{p_{z1}} - \frac{p_{x2}}{p_{z2}}\right)^2 + \left(\frac{p_{y1}}{p_{z1}} - \frac{p_{y2}}{p_{z2}}\right)^2} < 0.003 \\ |\frac{p_1 - p_2}{p_1}| < 0.05 \end{cases} \tag{10}$$

were considered as clones. From every clone pair the track with the largest number of hits was selected.

A track was identified as a muon if it had 3 muon hits attached ($lh_\mu > 0.001$) and if it had a transverse momentum $p_T^\mu > 0.7$ GeV/c. An electron candidate was required to deposit in the calorimeter a transverse energy $E_T > 1.$ GeV, to have ratio of the cluster energy to the momentum of the track $|E/p - 0.965| < 0.3$, and to have a bremsstrahlung cluster associated with the track.

The procedure of bremsstrahlung assignment is illustrated in fig.8. The search window is a rectangle with sides parallel to the axes x and y. The linear projection of the VDS segment to the ECAL surface defines one edge of the search window x_0. A cluster found in this position corresponds to bremsstrahlung emitted in front of the magnet. The original lepton cluster defines the second edge of the search window x_p. Clusters found between the 2 edges are considered as bremsstrahlung emitted inside the magnet. The vertical coordinates of the window is defined by the position of the first point. The size of the window is taken as:

$$y^{vds} + tg(\Theta_y)^{vds}(z^{clus} - z^{vds}) - y^{clus} < \begin{cases} 1.2 \text{ cm} & Inner \quad ECAL \\ 3. \text{ cm} & Middle \quad ECAL \end{cases} \tag{11}$$

which is three standard deviations of the difference between VDS projection and cluster position. The momentum of the lepton p_l is corrected for the energy of all clusters assigned as bremsstrahlung:

$$p_l' = p_l + \sum_i E_i \frac{x_i - x_p}{x_0 - x_p} \tag{12}$$

where E_i and x_i are the energy and position of the bremsstrahlung cluster, respectively.

6.2 $J/\psi \to \mu^+\mu^-$

For each unlike-charge muon pair the invariant mass is calculated. A clear J/ψ signal is observed. The background is described by a combination of like-charge muons (see fig.9). The signal is described by a Gaussian. The measured mean value of the mass is 3.087 ± 0.001 which is significantly lower than the tabular value 3.097. The width is wider than predicted by MC: 56 ± 1 versus 40 ± 0.4 MeV/c^2. Both effects can be explained by misalignment in the detector[3] [14].

The additional cuts applied are :

[3] In [24] was shown that the artificial squeezing of VDS by 0.15% or rotation around axis z by less that 0.5 mrad is enough to explain the difference of the J/ψ parameters in MC and data. However, one has to be aware of other possible sources of the difference.

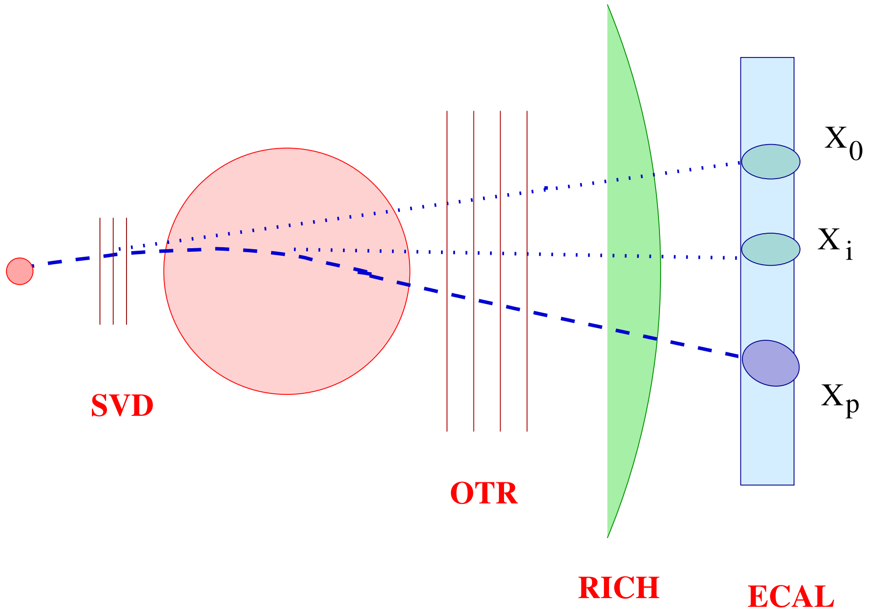

Figure 8: Bremsstrahlung reconstruction. The dashed line shows the track of the lepton. The dotted lines correspond to bremsstrahlung photons.

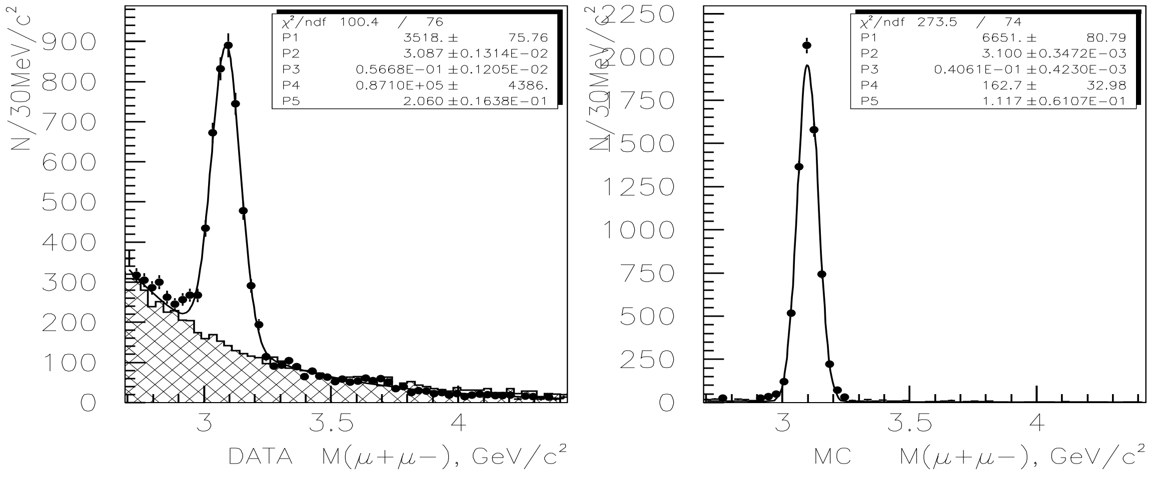

Figure 9: The invariant mass of $\mu^+\mu^-$ candidates shown for the data and MC samples. The hatched histograms represents the invariant mass of the pairs of muon candidates with the same charge.

- 2 and only 2 muon candidates per event.
- The J/ψ vertex is positioned on one of the targets: $|Z(J/\psi) + 4.91| < 1$ cm, $|Z(J/\psi) + 1.55| < 1$ cm
- the χ^2 probability of the di-muon vertex is restricted to $Prob(J/\psi\ \ vertex) > 0.005$
- The cut on J/ψ mass is $|M(l^+l^-) - M_0(J/\psi)| < \Delta M(J/\psi)$. The parameters are summarised in the tab.7.

Sample	$M_0(J/\psi)$	$\Delta M(J/\psi)$	$\varepsilon(\Delta M)$
μ-C	3.087	0.108	95.5%
μ-Ti	3.089	0.1188	95.7%

Table 7: The cut applied on invariant mass of the $\mu^+\mu^-$ combinations. The last column shows the efficiency of the given cut.

- Additional restrictions on $p_T(\mu)$, lh_μ or vertex do not improve $S/\sqrt{D}$ ratio.

The efficiency of the presented cuts is estimated using data as well as MC samples (see tab.8). The invariant mass of J/ψ events passed the above criteria is shown in fig.10 separately for the μ-C and the μ-Ti data.

Cut	MC		DATA	
	direct J/ψ	non-direct J/ψ	all J/ψ	background
Reconstruction	$94.3 \pm 0.1\%$	$94.4 \pm 0.1\%$	-	-
exactly 2 μ in event	$95.0 \pm 0.2\%$	$94.9 \pm 0.3\%$	$96.4 \pm 0.3\%$	89%
Z of vertex	$100. \pm 0.02\%$	$100. \pm 0.02\%$	$99.8. \pm 0.1\%$	99.6%
$Prob(vertex) > 0.005$	$97.2 \pm 0.1\%$	$96.9 \pm 0.2\%$	$92.6 \pm 0.5\%$	77%

Table 8: The efficiency of the different muon cuts estimated on the MC sample (NRQCD model) and the measured data. The MC efficiency is shown for the direct and non-direct J/ψ . The last column corresponds to the efficiency of the background under the J/ψ signal. The difference in efficiency of the cut on vertex χ^2 is explained by underestimation of the lepton momentum errors on data.

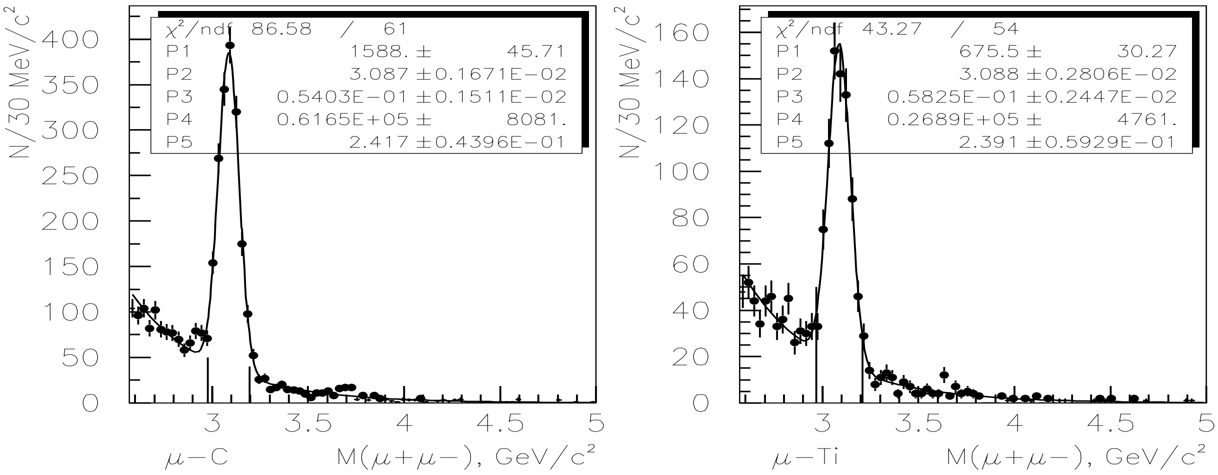

Figure 10: Events passing the selection cuts for $J/\psi \to \mu^+\mu^-$. Left: μ-C. Right: μ-Ti. The lines indicate the limits of the cut on the J/ψ mass.

6.3 $J/\psi \to e^+e^-$

The invariant mass of oppositely charged electron candidates for the entire data sample is shown in fig.11 The shape of the signal can be described by the function:

$$\frac{dN_{J/\psi}}{dM} = N_{J/\psi} \frac{2}{\sigma_M \cdot (\sqrt{2\pi} + \pi\sigma_{br})} \cdot \begin{cases} e^{-\frac{(M-M_0)^2}{2\sigma_M^2}}, & M > M_0 \\ \frac{1}{1+\left(\frac{M-M_0}{\sigma_M \sigma_{br}}\right)^2}, & M < M_0 \end{cases} \tag{13}$$

where $N_{J/\psi}$ is the total number of J/ψ , M_0 is the position of the maximum (equivalent to the mean of the Gaussian), σ_M is the width of the Gaussian, related to the detector resolution, and σ_{br} takes into account the detector resolution and the radiative losses of the leptons. This shape describes the MC distribution accurately (see fig.11b). Although large bremsstrahlung losses in the medium can be recovered by the bremsstrahlung reconstruction, small continuous energy losses in the medium by electrons and positrons are lost for reconstruction. The momentum resolution suffers from these losses as well.

A Gaussian is not adequate to describe the signal description in this case (fig.12). A fit with eq.13 yields $N_{J/\psi} = 3960 \pm 64$ for the MC sample of 3956 J/ψ , while the Gaussian results in $N_{J/\psi} = 3460 \pm 59$. The fit of the data signal with eq.13 gives $N_{J/\psi} = 1934 \pm 74$ while a Gaussian results in 1625 ± 61 events.

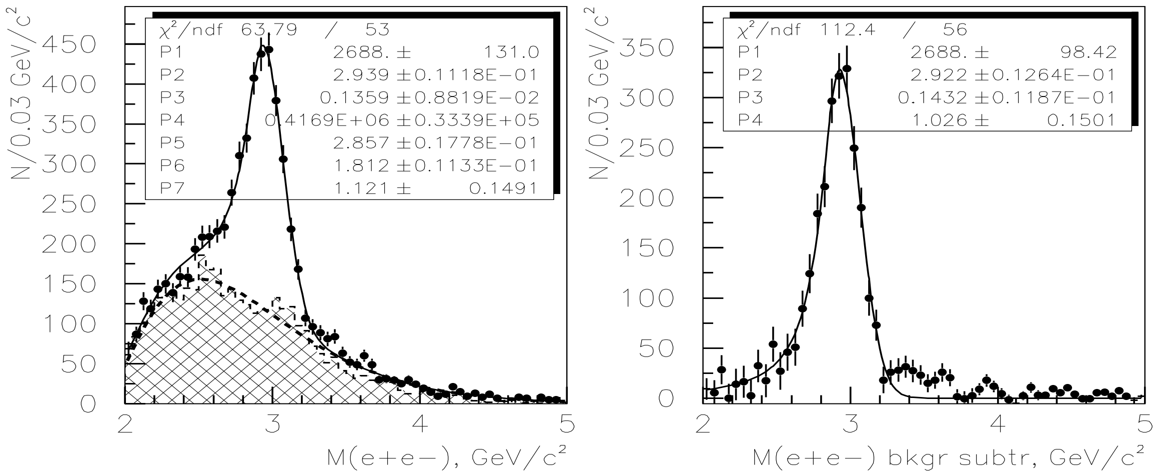

Figure 11: The invariant mass of the electron candidate pairs. a) Distribution obtained with the full statistics, the hatched histogram shows the background (see text for details); the parameters of eq.13 are $P1 \equiv N_{J/\psi}$, $P2 \equiv M_0$, $P3 \equiv \sigma_M$ $P7 \equiv \sigma_{br}$ while P4-P6 correspond to the background function. b) The invariant mass e^+e^- after the subtraction of the background. Here the parameter $P4 \equiv \sigma_{br}$ while the others are the same as before.

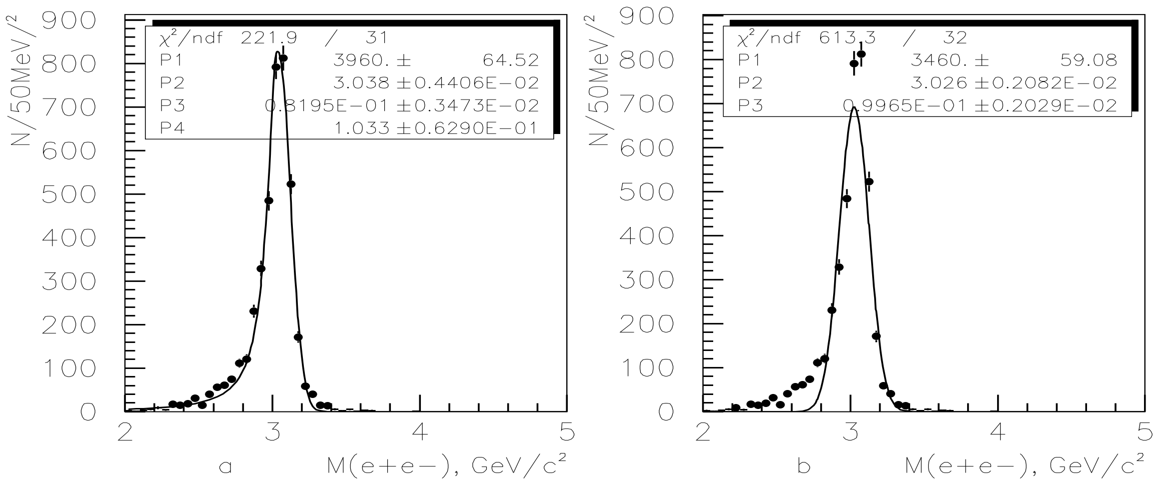

Figure 12: MC: invariant mass of e^+e^- pairs. a) Fit with equation 13; b) Fit with a Gaussian

The background can be described with a *fake bremsstrahlung* method [25]. In the main stream analysis we identify electron as a track with an additional cluster (real brem) associated. Then let us assume that the occupancy of the ECAL is symmetrical with respect to the axis y. If we search for a cluster with the same vertical coordinate y but with the opposite horizontal coordinate $-x$ we will find the same number of random combinations track-brem as on proper side but 0 correct brems. Let us consider the combinations with one (N_{rf} - for positive charged track, N_{fr} for negative one) or two (N_{ff}) fake bremsstrahlung assuming there are $N_{h^\pm}$ positive and negative charged hadrons; N_{e^+} positrons and N_{e^-} electrons:

$$\begin{aligned} N_{rf} &= (N_{h^+}\varepsilon_{h^+} + N_{e^+}\varepsilon_{e^+})(N_{h^-} + N_{e^-})\varepsilon_{h^-} \\ N_{fr} &= (N_{h^+} + N_{e^+})\varepsilon_{h^+}(N_{h^-}\varepsilon_{h^-} + N_{e^-}\varepsilon_{e^-}) \\ N_{ff} &= (N_{h^+} + N_{e^+})\varepsilon_{h^+}(N_{h^-} + N_{e^-})\varepsilon_{h^-} \end{aligned} \tag{14}$$

where $\varepsilon_{h^\pm}$ stands for the probability to assign a random cluster for positive or negative tracks as a bremsstrahlung while $\varepsilon_{e^\pm}$ is an efficiency of correct bremsstrahlung reconstruction. In this case the background of the uncorrelated hadrons or electrons will be:

$$N_{rr} = (N_{h^+}\varepsilon_{h^+} + N_{e^+}\varepsilon_{e^+})(N_{h^-}\varepsilon_{h^-} + N_{e^-}\varepsilon_{e^-}) = \frac{N_{rf}N_{fr}}{N_{ff}} \tag{15}$$

As one can see from Fig. 11 the given ansatz describes well the J/ψ sidebands. Unfortunately, when the statistics is small the distribution N_{ff} contains very few events, leading to large errors for N_{rr}. In this case, the following parametrisation:

$$N_{rr} = P_4(M - P_6)^2 e^{-P_5 M} \tag{16}$$

is used. On the complete statistics the discrepancy of the fits based on the parametrization and the fake bremsstrahlung background does not exceed 5% (see fig.11. We include this value as an additional uncertainty on the $N_{J/\psi}$.

The additional cuts applied to $J/\psi \to e^+e^-$ samples are :

- 2 and only 2 electron candidates per event.
- The J/ψ vertex is positioned on one of the targets: $Z(J/\psi)+4.91| < 1$ cm, $|Z(J/\psi)+1.55| < 1$ cm
- the χ^2 probability of the di-electron vertex is restricted to $Prob(vertex) > 0.005$
- The parameters of the cut on the mass of J/ψ $|M(l^+l^-) - M_0(J/\psi)| < \Delta M(J/\psi)$ are shown in tab.9.

Sample	$M_0(J/\psi)$	$\Delta M(J/\psi)$	$\varepsilon(\Delta M)$
e-C	2.98	0.312	85.7%
e-Ti	2.98	0.312	80.3%

Table 9: Cut on invariant mass of the e^+e^- combinations. The last column shows the efficiency of the cut. The difference in efficiency for the two samples is explained by the different parameters of the J/ψ mass distribution obtained on data.

- No additional cuts on the E_T^{clus}, E^{clus}/P of the lepton are applied.

The efficiencies of the presented cuts are estimated using data as well as the MC sample (see tab.10).

Cut	MC		Data	
	direct J/ψ	non-direct J/ψ	all J/ψ	background
Reconstruction	$93.3 \pm 0.1\%$	$93.4 \pm 0.2\%$	-	-
2 bremsstrahlung γ's	$18.1 \pm 0.7\%$	$18.4 \pm 0.9\%$	$19.8 \pm 2\%^*$	2.2%
exactly 2 l /event	$96.8 \pm 0.3\%$	$96.8 \pm 0.4\%$	$97.7 \pm 0.3\%$	98%
Z of vertex	$100. \pm 0.04\%$	$100. \pm 0.05\%$	$99.3 \pm 0.2\%$	98%
$Prob(vertex) > 0.005$	$98.2 \pm 0.2\%$	$97.0 \pm 0.4\%$	$88.1 \pm 0.7\%$	78%

Table 10: The efficiency of the different restrictions, shown for MC (direct J/ψ or χ_c events) and for experimental data. The last column shows the rejection of the background under J/ψ signal. *) The efficiency of the bremsstrahlung cut estimated on data is taken from [26].

The results of the fit procedure for events from e-C and e-Ti samples are shown in fig.13. The parametrization agrees with the background description obtained by the fake bremsstrahlung method. The position of the signal is shifted with respect to the tabular value by about 180 MeV/c^2. From the eq.6 we can expect that the position of χ_c signal will be increased by about 20 MeV/c^2.

7 Charged and Neutral Multiplicities.

The occupancy of the detector is an important issue in the analysis of the χ_c . On one hand, a higher occupancy of the calorimeter leads to a higher combinatorial background

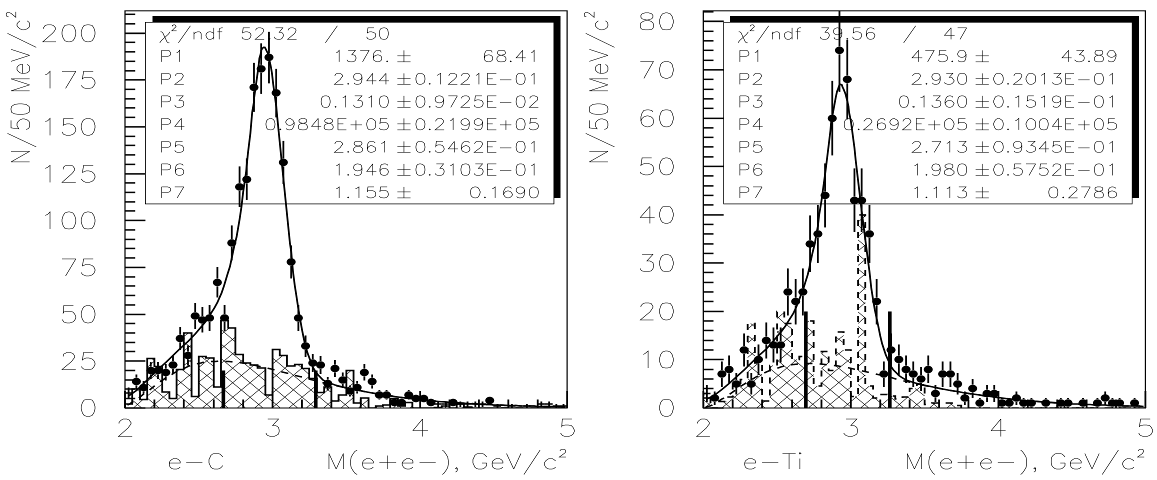

Figure 13: The invariant mass distribution of the selected combinations e^+e^- for the C and Ti samples. The fit corresponds to the sum of eq.13 and eq.16. The hatched histograms show the fake bremsstrahlung background. The lines correspond to the mass window applied for the χ_c analysis.

under the χ_c . On the other hand one has to be careful with cuts on the occupancy since it is directly connected with the multiplicity of the event and might depend on the physics of event. As it was discussed in [27], processes with a small cross section (e.g J/ψ production) happen with largest probability in *central collisions*. Events with large cross section - such as inelastic scattering - happen every time the proton hits a nucleus, even if it is not a central collision. In a central event the proton traverses the longest path through the nucleus and creates more particles than on a shorter path. As a result, a J/ψ event is accompanied by a larger number of particles than a minimum bias event. The comparison of the multiplicity of J/ψ and minimum bias events confirms this hypothesis [27]. Since the cross section of the direct J/ψ is of the same order as χ_c production both types of events should have similar multiplicity excluding the decay products of charmonium.

Another possible source for different Multiplicities in J/ψ events is the energy of the hard gluon produced together with charmonium. Again the direct J/ψ and χ_c events have similar gluon characteristics.

One can thus expect that the particle multiplicity of direct J/ψ and χ_c events are similar. The systematic error due to this assumption is checked in sec.10 by cuts variation. The difference in the one photon in case of χ_c is negligible.

The multiplicity of charged particles is taken to be proportional to the number of the tracks in VDS (N_{vds}), whereas the neutral multiplicity is estimated as the number of clusters with energy $E_{clus} > 5$ GeV (N_{clus}) [4]. The values N_{vds} and N_{clus} are correlated as shown in fig.14. J/ψ and background events have different occupancy as shown on fig.15.

In spite of the correlation it is worth to optimise the cuts on both variables. An upper limit on N_{vds} reduces the background under the J/ψ signal (possible ghosts of the trigger) while an upper limit on N_{clus} allows to reduce the combinatorial background under χ_c . The cuts were optimised for each sample separately (see tab.11).

	$< N_{clus} >$	UL N_{clus}	$\varepsilon_{N_{clus}}$	$< N_{vds} >$	UL N_{vds}	$\varepsilon_{N_{vds}}$	ε_{tot}
μ-C	8.41	19	97%	21.09	30	87%	86%
μ-Ti	10.10	19	97%	23.85	34	79%	79%
e-C	13.81	19	91%	22.76	30	81%	77%
e-Ti	14.08	19	94%	26.05	34	77%	74%

Table 11: The average charged and neutral multiplicity of J/ψ events; the upper limits applied in the analysis and the efficiency of the cuts.

8 Photon reconstruction.

The photon was reconstructed as a cluster in the ECAL. Here we will discuss the problems connected with photon reconstruction such as position of the dead channels, energy resolution, cluster shape, cluster-track relation and occupancy of the ECAL. At the beginning a short explanation of the energy reconstruction by the calorimeter and the its simulation are given.

Energy reconstruction in the calorimeter. The signal measured by the calorimeter electronics is proportional to the energy deposited in the corresponding cell. It is expressed in *ADC counts* with a constant offset called the *pedestal*:

$$E = C \cdot ADC - Ped \tag{17}$$

[4]In fact the N_{clus} includes part of the charged multiplicity as well. We are not able to eliminate the fraction due to missing data from ITR. In addition, the part of the photons from primary vertex convert behind magnet and therefore is identified as cluster-track pairs.

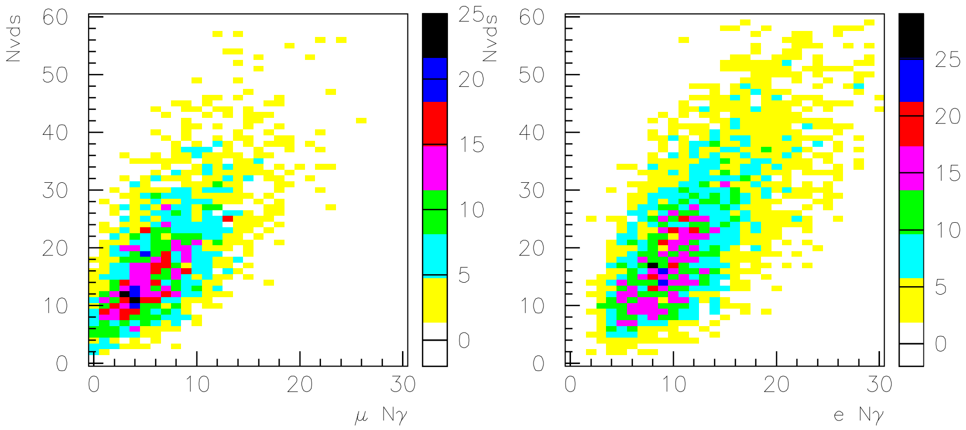

Figure 14: The correlation of the charge and the neutral multiplicity. All events shown corresponds to the J/ψ mass window. The left plot contain all muon events passed cut on J/ψ , the right plot is sum over all electron events passed the cuts.

The coefficient C relates the adc counts with the energy in GeV (see [28], [29] for the calibration procedure). On average it is around 30 MeV/adc for the Inner and 15 MeV/adc for the Middle part of the ECAL. Both the calibration constants C and the pedestal values Ped are known with some precision which is estimated on data for each run period and saved into the database. The KEYTABLE 17 calibration tables were used. Correlated noise (the pedestals of neighbouring channels oscillate synchronicaly) is eliminated using a noise suppression mechanism[16].

The reconstruction program performs the search of the local maxima in the energy-position spectrum of ECAL channels. Found cells and their 8 adjacent neighbours are combined into a cluster. The reconstruction of the cluster is done by the CARE package within ARTE-03-09-r5 [30].

Low energy clusters reconstructed in *MIP* mode on the prolongation of charged tracks were removed. Such clusters have a typical value for the transverse energy of $E_T < 0.1$ GeV. Clusters associated with leptons from the J/ψ were not accepted as photon candidates.

Simulation of the ECAL response. In the analysis of a MC event, the energy of all particles deposited in each ECAL cell is summed up, digitised and reconstructed, as it is done for real data. During digitisation the simulated energy deposit in the cells is transformed

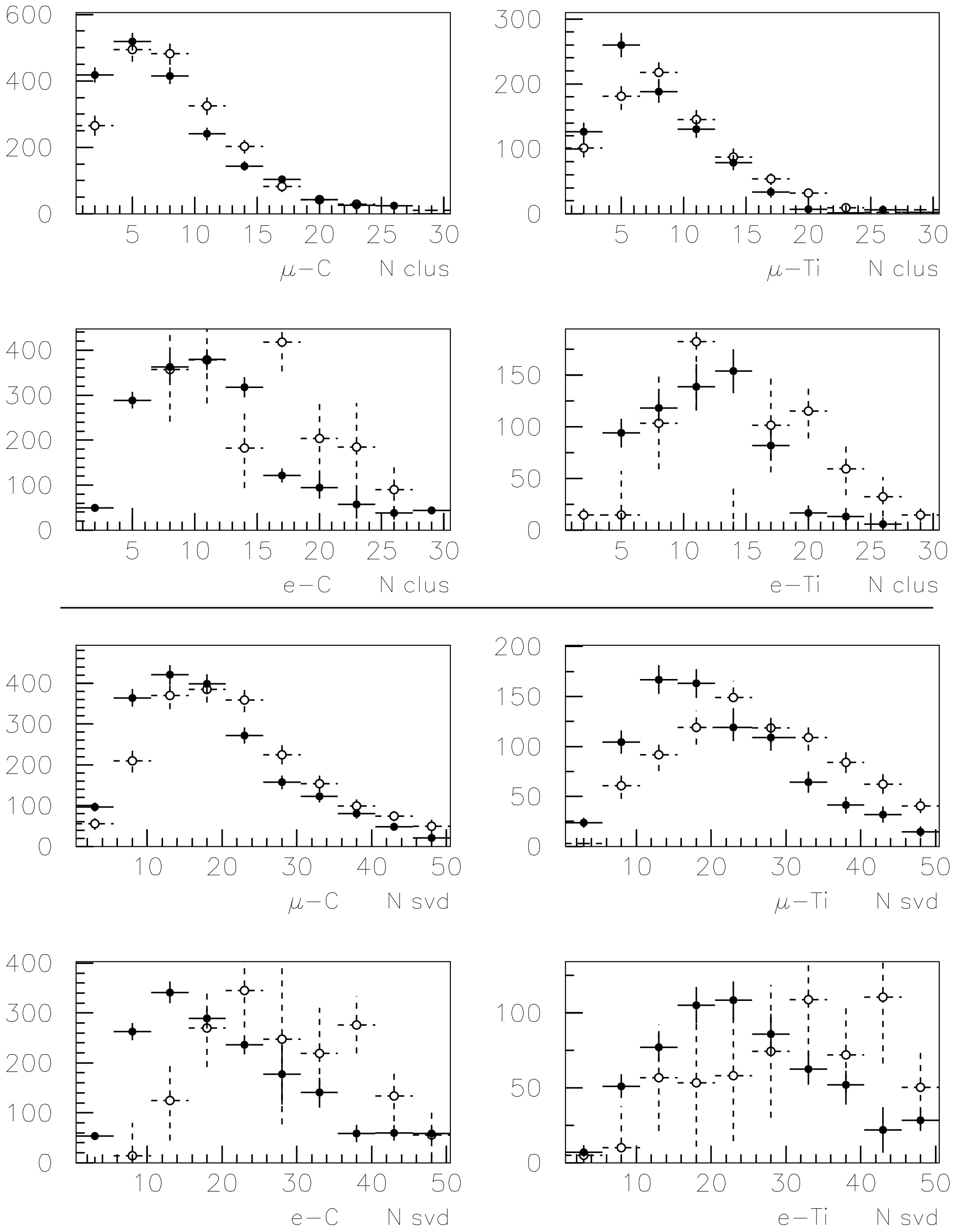

Figure 15: The multiplicity in the J/ψ events. The upper two rows show N_{clus}. The lower two rows show N_{svd}. The multiplicity is shown for each sample separately. The filled points are the number of J/ψ obtained via the fit of the number of J/ψ in each bin. The open circles are the spectrum of the events with $M(\mu+\mu-) > 2.5\mathrm{GeV/c^2}$, $M(e+e-) > 2.\mathrm{GeV/c^2}$ with the J/ψ spectrum subtracted (background). The background histograms are normalised to the integral of the J/ψ histograms.

into adc units $ADC = C' \cdot E_0$. The inverse calibration constants C' for each ECAL channel were generated in a Gaussian distribution of mean inverse to the calibration constants $1/C$ and variance δC estimated on the data. To each channel the measured pedestal distribution was added. For the channels with very wide pedestals ($\delta Ped > 10\ adc$) which are known to be non-Gaussian, the tails of the distribution were cut away. No signal was associated with the channels which were switched off in the data analysis. The ECAL maps of dead channels, calibration constants and pedestals values for the run 16665 were taken as basis for the simulation. In addition, correlated noise was simulated for each event according to a Gaussian distribution with a width of 1 adc count.

Finally the complete reconstruction chain was applied in the same way as for experimental data. The noise suppression algorithm was switched on as well for the muon MC.

Definition of the MC origin of the cluster. For analysis purposes the cluster which corresponds to the photon from a χ_c has to be identified. Since the electro-magnetic shower can start in front of the ECAL it is not enough to check the ECAL energy deposit by the photon. The decay products (e.g. leptons from conversion or decay products of these leptons) should be considered as well if they deposit energy in the same place.

To relate photons from the primary vertex (e.g. from the decay $\chi_c \to J/\psi\gamma$) and the ECAL cluster the following procedure is used. The photon or its decay products were required to deposit together at least half of the photon original energy in the given cluster $E_{clus}/E_{MC} > 0.5$. Here the decay is required to happen after the plane $z = 550$ cm. In case the decay happens before $z = 550$ cm the photon is supposed to be lost for the reconstruction. In case another particle deposits in the same place more energy than the given photon the cluster is not assigned to the photon.

8.1 Position of the dead and hot channels.

During the year 2000 run the readout and pretrigger boards of the ECAL were not completely equipped. Some of the boards were not used in the data acquisition during the complete period. Such boards are easily recognised in the occupancy plot of the ECAL (see fig.16). Nine readout cards which were missing in some runs (more than 20% of the period) were excluded from the analysis altogether. The other boards worked stably.

The stability of the channels in the accepted readout boards was found to be satisfactory. The amount and position of the dead channels (white spots on the occupancy plot) did not change from run to run for the period June to August in more than 98% cases.

Some channels exhibited extreme behaviour (*hot* or *cold*) with respect to the neighbours. To select such channels each period was divided into several parts. In case the occupancy of a channel deviated more than five standard deviations from the occupancy of its neighbours for several parts of the period, the channel was rejected. In total 10 channels were rejected, six of them were hot during the entire period. This procedure removes hot spots in the distribution of photon candidates[5], whereas the parameters of the observed signal was not affected.

No cluster can be created with its center at the place of a dead channel. In case the dead channel is bordering the central cell the position of the cluster and the energy is affected. The clusters with two dead channels bordering the central cell (*incomplete clusters*) are not considered. In case the cell is located in the corner of the cluster the relative contribution of the cell to the cluster is very small and can be neglected.

Since the electronics of the OUTER part of calorimeter was being installed and the π^0 calibration was not yet performed there, the data from the OUTER part of the ECAL were not used in this analysis.

8.2 Restriction on the energy of the cluster.

To decide on the restriction on the energy of the cluster one has to consider the following problems. First, the sample of low energetic clusters is contaminated by the background of soft secondary particles and artificial clusters due to wide pedestals. Clusters with an energy below 2 GeV are difficult to reconstruct, the energy and position resolution is poor. On the other side, the average energy of a photon from a χ_c which passed the trigger is about 7 GeV. In order to obtain a reasonable efficiency one has to consider all clusters with energies down to a few GeV (see fig.17).

The solution can be found in the analysis of the background shape under the χ_c signal. As is visible from fig.18 clusters with an energy up to 2 GeV contribute significantly only to the lower part of the spectrum. In case the energy threshold is increased to 4 GeV, the background peaks in the vicinity of the χ_c signal. The χ_c sidebands are significantly reduced with respect to the χ_c interval resulting in large uncertainty in the normalisation of the background. The threshold chosen is $E_{clus} > 3.$ GeV for all samples.

The same holds for the cut on the transverse energy of the cluster.

[5]The search of the hot channels was performed before the noise suppression algorithm was applied. After the noise suppression few additional channels with extreme behaviour were found. These additional channels were removed after the reconstruction of the clusters was performed.

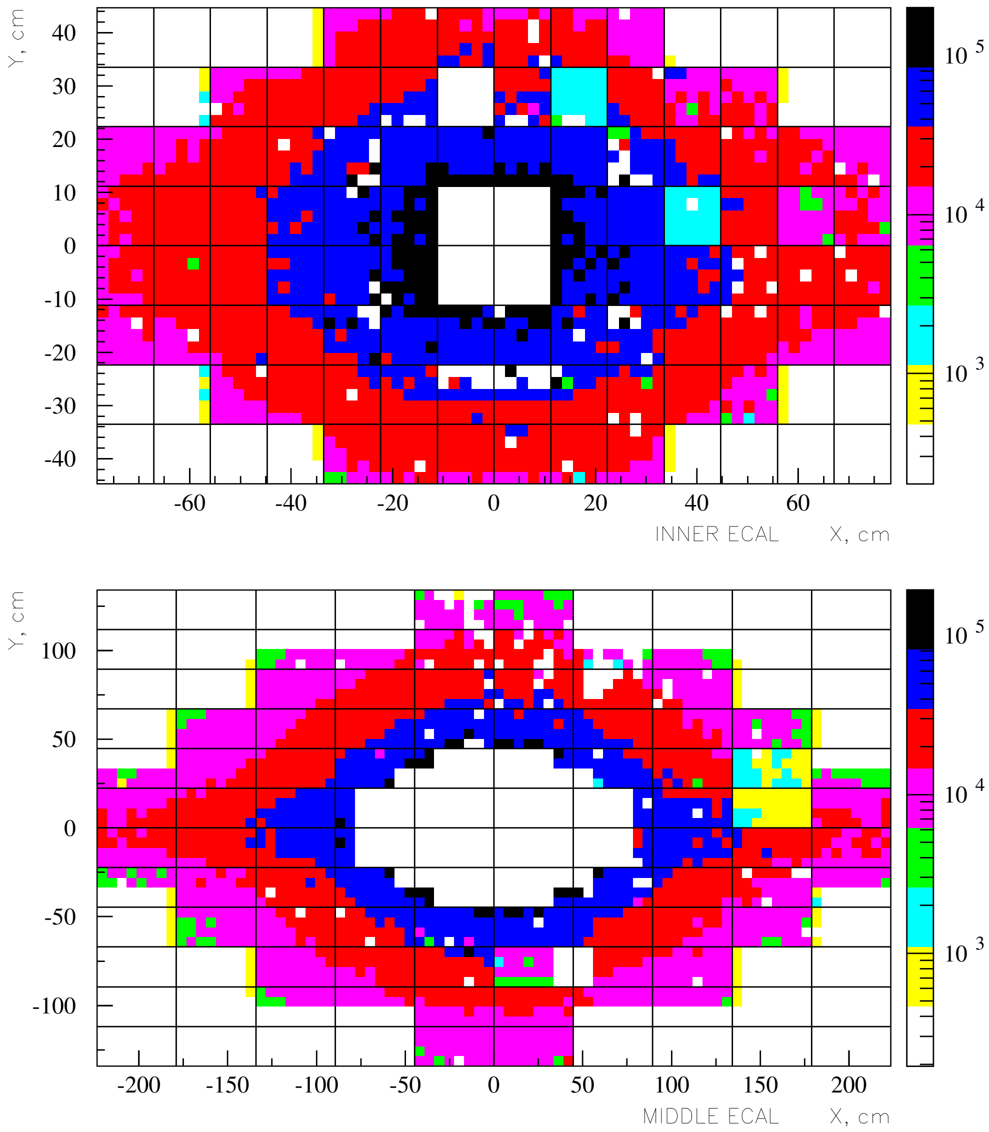

Figure 16: The occupancy of the ECAL clusters for the July period integrated over all types of the events. The INNER (upper plot) and MIDDLE (lower plot) calorimeter parts are shown.

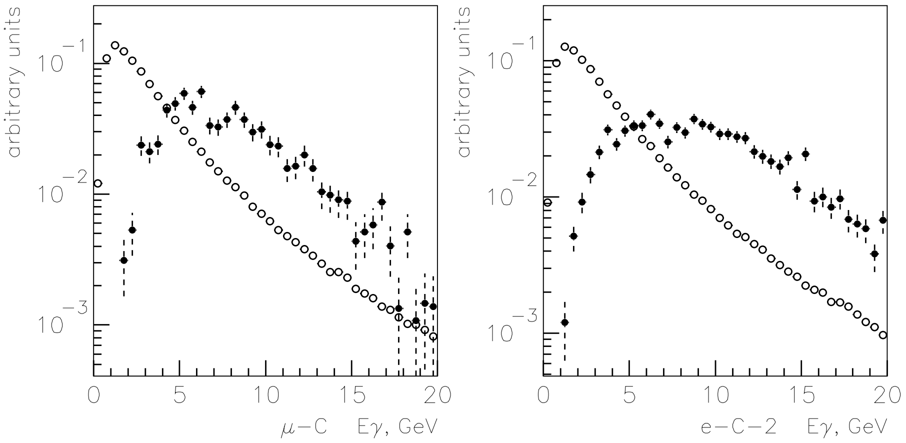

Figure 17: The cluster energy spectra. a) empty circles: all clusters from the subsample $\mu - C$; filled circles: MC spectrum of photons from χ_c events passed the muon trigger; b) empty circles: all clusters from the subsample e-C; filled circles: MC spectrum of photons from χ_c events passed the e-SLICER trigger. The integral of each spectrum is normalised to 1.

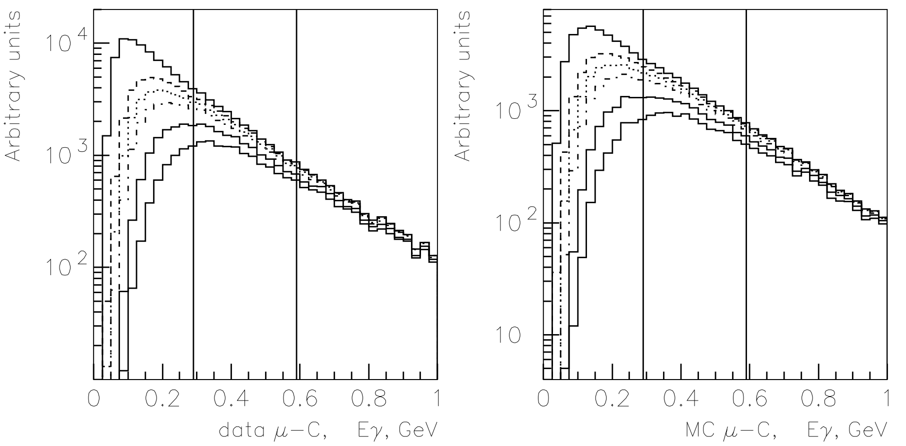

Figure 18: The dependence of the background shape on the E_{clus} threshold (from top to bottom: 0, 2., 2.5, 3., 4., 5. GeV). The left plot corresponds to the data sample μ-C, the right plot is MC.

8.3 Cluster shape analysis.

The granularity of the ECAL is larger than the Moliere radius of the medium of the corresponding modules. A large fraction of the energy of the electron or photon is deposited in one cell unless the particle hits the border between the cells. In contrast, hadronic clusters are spread out and asymmetric. Due to the correlated pedestals fake clusters might occur. Most likely, they have similar energy deposition in several cells, in contrast with electro-magnetic clusters.

The ratio of the central cell energy to the total cluster energy (fig.19) provides a useful tool to reject the background. The optimal cut is $E_{centr}/E_{clus} > 0.6$ for all samples.

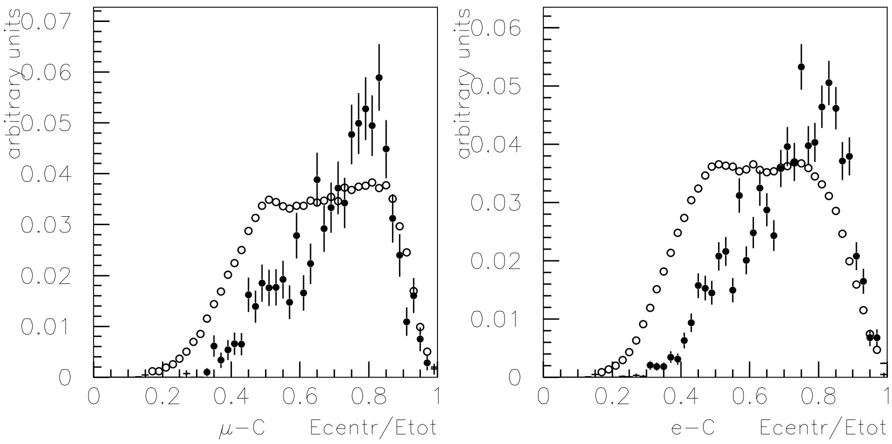

Figure 19: The ratio of the central cell energy to the total cluster energy. The filled circles shows the MC distribution for photons from χ_c decay while the empty circles corresponds to the cluster distribution taken from experimental data. The left plot shows distributions for the $\mu - C$ sample and the right one shows e-C. All histograms are normalised to 1.

8.4 Association of OTR tracks with clusters.

Since some clusters are caused by charged particles one can consider the relations between clusters and charged tracks in order to suppress background under χ_c signal. In 44% of all cases when the cluster can be associated with a photon from χ_c it is actually deposited by the leptons from the conversion which happens behind the magnet. Therefore the usage of such cut will significantly reduce the efficiency of the χ_c reconstruction. From fig.20 it is evident that this cut suppresses the background under the χ_c less than the χ_c signal itself. This cut is thus not applied.

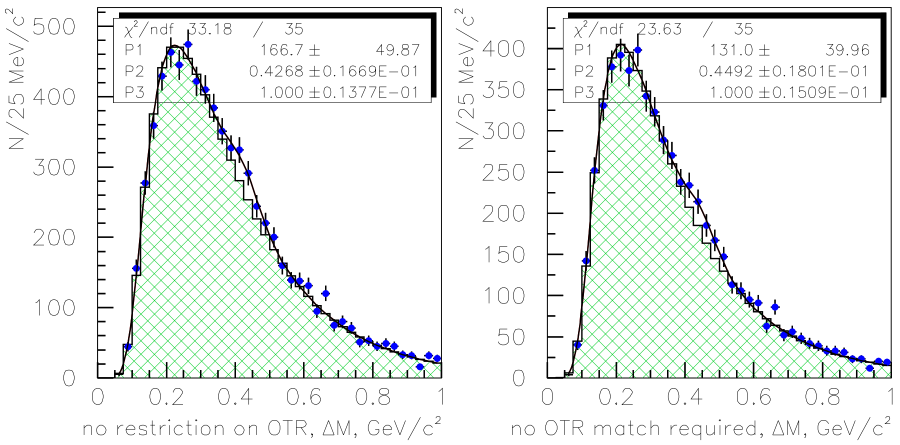

Figure 20: The ΔM distribution without (left plot) and with (right plot) a cut on OTR tracks associated with an ECAL cluster.

8.5 Occupancy of the area close to the beam pipe.

The area close to the beam pipe shows an occupancy of up to 30% of soft clusters[31]. Under such conditions the probability for the overlapping clusters and therefore for poor energy resolution is very high. To avoid this, the following restriction was implemented:

$$\frac{x_{clus}^2}{4} + y_{clus}^2 > 484\text{cm}. \tag{18}$$

The cut applied was checked on MC and data (fig.21). The loss in the N_{χ_c} of data (9%) agrees with MC loss of this cut (14%).

8.6 Efficiency of the photon reconstruction.

To estimate the photon reconstruction efficiency ε_γ the procedure applied to the measured data is repeated for all MC events containing a χ_c . The efficiency is defined as:

$$\varepsilon_\gamma = \frac{N_{\chi_c}^{MC}}{N_{J/\psi}^{MC}}, \tag{19}$$

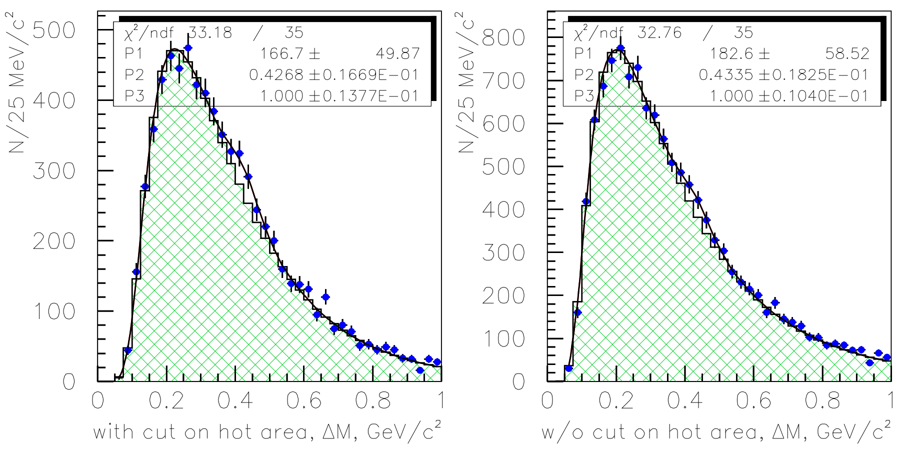

Figure 21: The ΔM distribution with and without cut on the hot area around the beam pipe.

where $N^{MC}_{\chi_c}$ is extracted from the fit of the χ_c signal and background and $N^{MC}_{J/\psi}$ is taken from the di-lepton mass distribution of χ_c events passing the cuts as it is done on data.

An example of the MC distributions are shown in fig.22.

The loss of events can be characterised as follows:

- Only 65% of the photons from χ_c hit the calorimeter and can be reconstructed. 44% of them suffer conversion behind the magnet.
- 79% of the reconstructed photons are found in the INNER and MIDDLE part. Dead and hot areas in the ECAL reduce the efficiency by 5%. Rejection of incomplete events results in an additional loss of 3%.
- The efficiency of the energy cut on the photon is 98%.
- The cut on the energy of the central cell allows 78% of the photons to pass.
- 86% of the photons survive the restriction on the area around the beam pipe.

Since the samples differ by kinematics and acceptance, the simulation and efficiency estimation is done for each sample separately. The results are summarised in the table 12. The systematic uncertainty in the estimation of the efficiency is discussed below (sec.10).

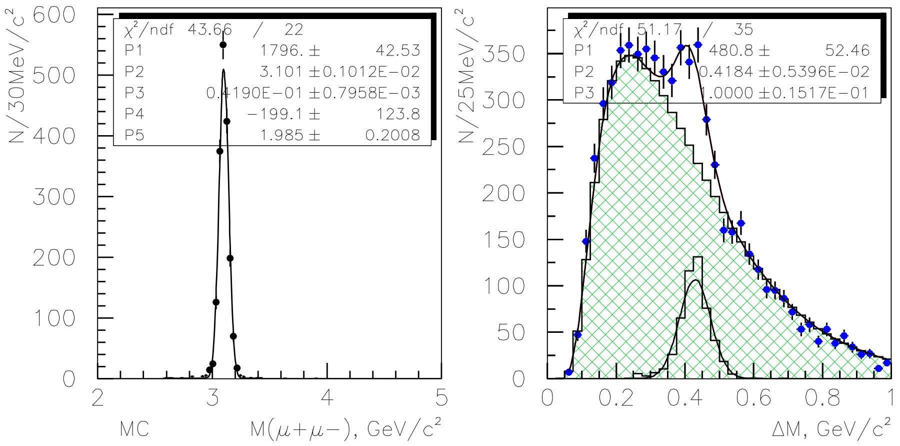

Figure 22: The χ_{c1} and χ_{c2} events weighted according to the NRQCD prediction are shown. The left plot is the di-muon invariant mass. The right plot is a combination of the all photon candidates and J/ψ from the χ_c events. The hatched histogram corresponds to the background of mixed events. The true combinations of photon and J/ψ from the χ_c decay are shown as the curve at the bottom.

Sample	$\varepsilon_\gamma(NRQCD)$	$\varepsilon_\gamma(CSM)$
μ-C	$26.5 \pm 1.1\%$	$25.9 \pm 0.8\%$
μ-Ti	$27.1 \pm 1.9\%$	$29.6 \pm 1.5\%$
e-C	$32.8 \pm 1.5\%$	$30.7 \pm 1.1\%$
e-Ti	$32.7 \pm 2.6\%$	$36.9 \pm 2.0\%$

Table 12: The total efficiency of the cuts applied to the photon for different production models.

9 The experimental results on the χ_c signal.

9.1 Invariant mass of the $J/\psi\gamma$ combination.

The invariant mass of all J/ψ and photon pair combinations for each subsample is shown on fig.23. The largest μ-C and e-C samples shows a clear signal with a significance of more than 3 standard deviations.

The signal is described by a Gaussian with fixed width (0.045 GeV/c^2). The number of events in the Gaussian and the mass are free parameters. For the background description the J/ψ and clusters from the different events are mixed. For the fit, the shape of the background is fixed, whereas its normalisation is a third free parameter. The number of mixed events is about 1000 times bigger than the original sample, so that the errors of the background description are negligible. During the fit procedure the rescaling of the background from the mixed events is used.

The shift of the signal in the electron samples with respect to the muon samples agree with the expectation based on the correlation of the δM and M_{ll} described in sec.2.1. After the correction of $0.123 \cdot (M_{ll} - 3.097)$ (see eq.6) is applied to δM on an event by event basis, the parameters of the mass agree. The sum of all four spectra is shown in the fig.24. The fitted number of χ_c agrees with the sum of the N_{χ_c} from the four samples.

Shape of the signal. In the invariant mass spectrum of J/ψ and photon candidates one would expect to see the sum of the two charmonium states: χ_{c1} and χ_{c2}. The simulation of each state results in a ΔM distribution of Gaussian shape with some additional tails due to losses in the detector or overlapping clusters. Since the resolution is of the order of the mass difference ($M(\chi_{c2}) - M(\chi_{c1}) = 40$ MeV/c^2) the combined distribution of both states is also well described by a Gaussian.

Background description. Let us consider the possible sources of the correlated pairs of J/ψ and photons other than decays of charmonium.

They could be produced in the decays of heavy mesons such as B-mesons, Υ or χ_b. Since the cross section of those mesons is very small we can neglect this source. The same holds for the correlated production of the J/ψ and charged particles which deposit a sufficient energy in the calorimeter.

The NRQCD predicts the cross section of the $\eta_c(2S)$, χ_{c0} and $\psi(2S)$ to be of the same order of magnitude as χ_{c1} or χ_{c2}. Since the decay branching ratios of these mesons to J/ψ and photons are more than 20 times smaller than $Br(\chi_{c2} \to J/\psi\gamma)$ they can be neglected in

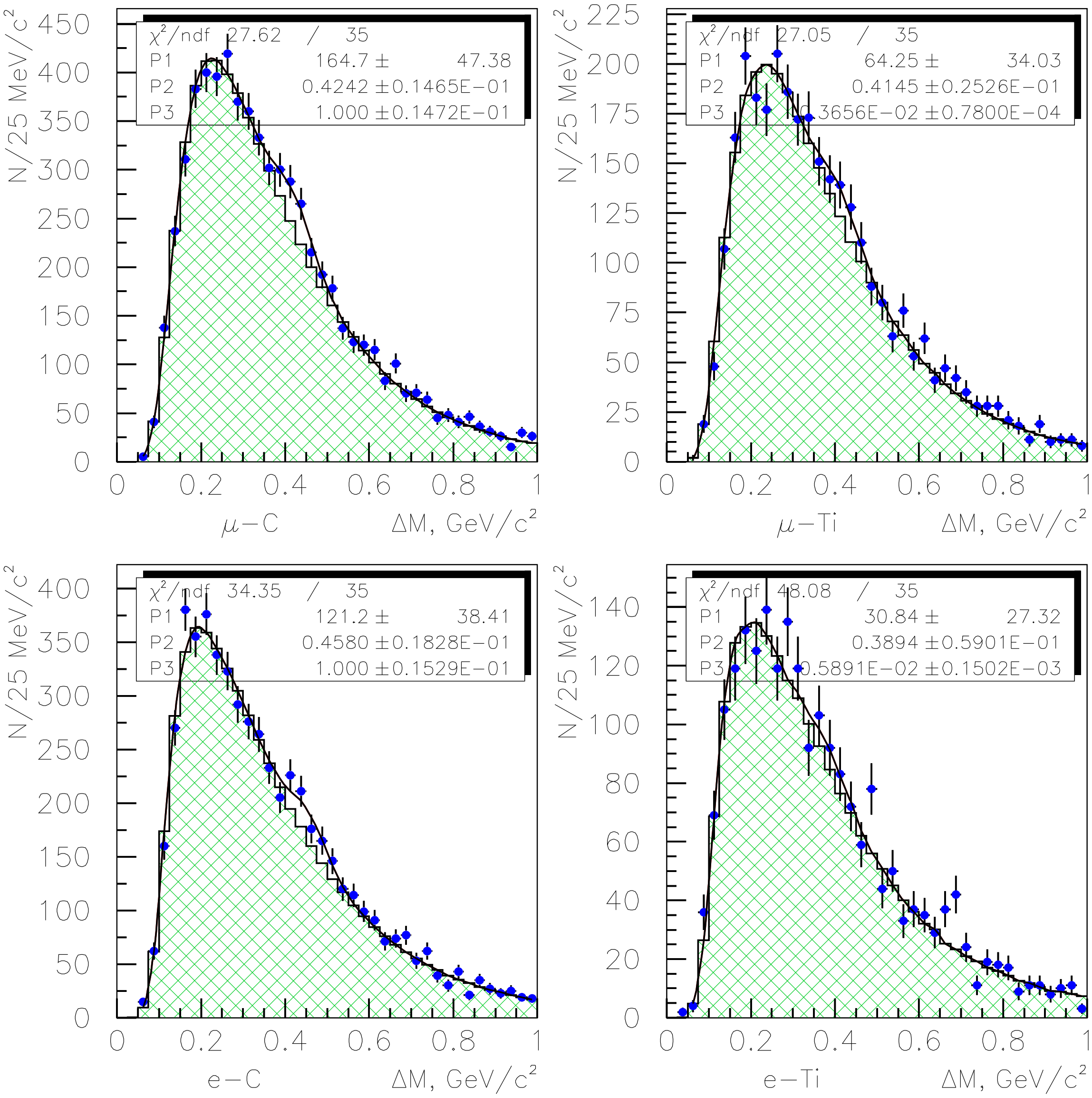

Figure 23: The ΔM distribution for each subsample. The normalised mixed events are shown as hatched histograms.

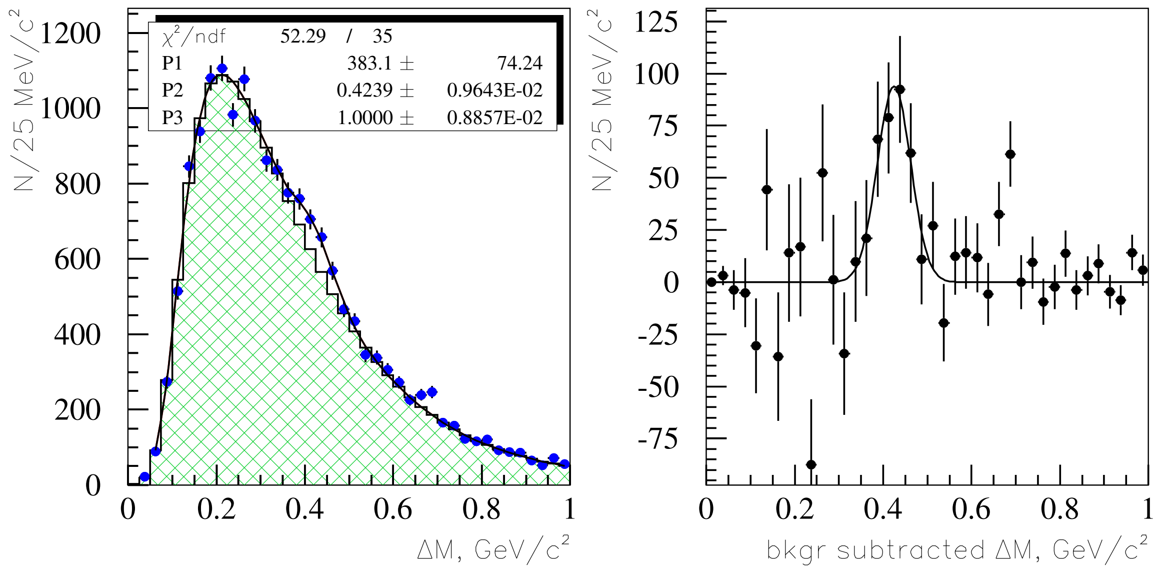

Figure 24: a) The ΔM distribution for entire sample. The normalised mixed events are shown as hatched histogram. b) ΔM distribution for entire sample with background subtracted. The line shows the Gaussian fit.

the present analysis. This is also supported by the fact that the production of these mesons with consequent decays into J/ψ and photons was not not observed in proton-nucleus interactions [7].

Another source could be the radiative correction to the decay vertex of the J/ψ : $J/\psi \to l^+l^-\gamma$. This photon is mostly directed along the momentum of one of the leptons and therefore would not be distinguishable from bremsstrahlung before the magnet. Clusters of this type are removed in the electron sample. In the muon sample, no excess of "bremsstrahlung" clusters was found on the prolongation of the muon track from J/ψ with respect to the muons from J/ψ sidebands. Therefore the fraction of such radiative decays is considered to be negligible.

The major part of the background is assumed to be uncorrelated random combinations of the J/ψ and clusters. The simulation of this background is done by combining all J/ψ and all clusters from different events passing the selection criteria (*mixed background*). To check whether this approach is correct, lepton pairs from the sidebands of the J/ψ ($0.18 < |M_{ll} - 3.085| < 0.5$ GeV/c^2) were taken and combined with clusters. The shape of these mixed events repeats the original background spectrum, justifying the assumption.

The probability of overlapping clusters is higher in events with high multiplicity than in those with small occupancy. As a result more low energetic clusters can be found in the former type. Fig.25b shows the contribution of events with low and high neutral multiplicity, respectively, to the background underneath the χ_c signal. The difference between the two spectra is small but not negligible. To insure the proper background description only events with the same number of the energetic clusters were mixed. The fraction of photons from events of different multiplicity is identical for direct and mixed spectra. The charge multiplicity of the events is not significant for the background description since the J/ψ kinematics is about the same.

The spectra of p_x, p_y, p_z J/ψ momenta were checked, as well as the position and the energy of the photon candidates, in order to ensure that no detector effects cause the peak in the ΔM distribution. The angular distribution of the combination of J/ψ and clusters agrees with MC expectation.

The mixed background method works on MC as can be seen from fig.22.

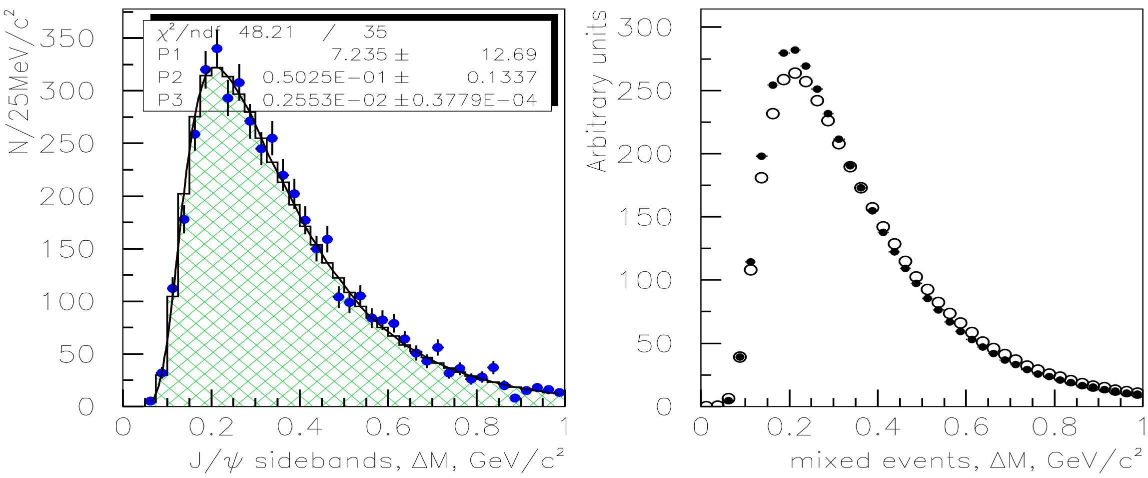

Figure 25: a) Δ_M distribution for pair of leptons with invariant mass $0.18 < |M_{ll} - 3.085| < 0.5$ GeV/c^2 (points). The hatched histogram represents the mixed background. b) Mixed event combinations with different occupancy: black points with $N_{clus} <= 6$, empty circles with $N_{clus} > 6$.

10 Study of the uncertainties.

Here we study the systematic uncertainties in the determination of $N_{J/\psi}$, N_{χ_c} and ε_γ.

Model dependence. As was discussed above the kinematic parameters of the photon and J/ψ are different in the NRQCD and the CSM models, as does the photon reconstruction efficiency. However, the ratio of the trigger efficiency of χ_c and direct events is close to 1 in both cases. The variation, which does not exceed 4%, is regarded as systematic uncertainty for the acceptance. The two mentioned uncertainties correlate, and the total systematic uncertainty for both together is estimated to be 4%.

In the CEM model the J/ψ kinematic distributions are similar to NRQCD (within a few percent) within the HERA-B acceptance [9]. The difference between the direct and non-direct J/ψ spectra is insignificant. The photon momentum in the c.m. system is equal to J/ψ . Consequently if the J/ψ spectra are identical in the CEM and NRQCD models, the photon kinematics is similar as well. We assume that the difference does not exceed 5%.

Misalignment and lepton momentum measurement. The inefficiency due to misalignment was found to be negligible. As was shown in [24] the possible sources and sizes of misalignment are strongly restricted by the parameters of the J/ψ . The χ_c signal was found to be insensitive to this level of misalignment. The same holds for the accuracy of the momentum measurement of the leptons. The systematic change of the momentum by a few percent in equal or opposite directions affects neither the MC nor data χ_c signal.

Material in the detector. In the analysis we rely on the correct description of the amount of material in the simulation of the detector which determines the probability of photon conversion. Photons which convert in the vertex detector or in the magnet are essentially lost for the reconstruction via ECAL clusters. Exact knowledge of these losses together with the kinematics of the photon and the performances of the ECAL defines the efficiency of the photon reconstruction.

We can verify the amount of material in the detector by a comparison of the bremsstrahlung recovery efficiency ε_{brem} on MC and data. ε_{brem} reflects the probability $p(x)$ of bremsstrahlung to be emmited combined with the bremsstrahlung survival probability $S(x)$ and with the probability $r(x)$ to register both electron and bremstrahlung as function of the emmision point x and can be written as:

$$\varepsilon_{brem} = \int_0^A p(x)S(x)r(x)dx = R\int_0^A \lambda e^{-\lambda(A-x)}dx = R(1-e^{-\lambda A}). \tag{20}$$

assuming that the material is distributed homogeneously and that p(x) is a constant, $p(x) = \lambda$. Again only the bremsstrahlung emmision and the conversion in front or inside the magnet affect ε_{brem} while same processes behind the magnet affect the space and energy resolution of the cluster. The limit of integration A is the end of the magnet area. In first approximation the registration probability is independent of the x ($r(x) = R$).

The probability of a χ_c photon to deposit a cluster (according to the definition given in sec.8) is determined by the survival probability $S(x)$:

$$\varepsilon_\gamma^0 = 0.9e^{-\lambda A} \tag{21}$$

wherethe factor 0.9 is the fraction of photons from the triggered χ_c decay in the acceptance of the HERA-B . Combining eq.20 and eq.21 for data and MC one obtains

$$\varepsilon_\gamma^{0data} = 0.9 + (\varepsilon_\gamma^{0MC} - 0.9)\frac{\varepsilon_{brem}^{data}}{\varepsilon_{brem}^{MC}}\frac{R^{MC}}{R^{data}} \tag{22}$$

The ratio R^{MC}/R^{data} is assumed to be equal to 1. The deviation from 1 can be due to the different J/ψ kinematics or due to the performances of the ECAL which are considered in other paragraphs of this section. The values of the $(\varepsilon_{brem}^{data})^2$ and $(\varepsilon_{brem}^{MC})^2$ are given in the tab.10 as "2 bremsstrahlung γ's". The numbers are compatible within one standard deviation. On the basis of the error on the $(\varepsilon_{brem}^{data})^2$ we extract the relative uncertainty on the ε_γ^0 of 2% according to eq.22.

Miscalibration of the ECAL. The calibration of the ECAL is an important issue for the χ_c analysis. The π^0 analysis[29] of the year 2000 data showed that there is no systematic shift in the π^0 mass and, therefore, in average the reconstructed energy of the cluster is equal to the incident energy. The effect of the miscalibration (uncertainty in the determination of the constants C from eq.17) leads to a widening of the π^0 signal. The miscalibration level is estimated to be 5-10% for all ECAL channels. The effect of the miscalibration on the χ_c signal was studied with Monte Carlo. As it is shown in fig.26 the most affected value is the width of the χ_c . The number of the reconstructed events and the mass are practically unchanged. For a miscalibration of between 5 and 10%, the width of χ_c is about 42-46 MeV/c^2. The systematic uncertainty can be estimated from fig.26 as variation of the ratio $N_{\chi_c}/N_{\chi_c}^0$, where N_{χ_c} and $N_{\chi_c}^0$ are the observed and expected number of χ_c .

Correlated noise in the ECAL. During the year 2000, correlated noise in the ECAL was observed, which caused a synchronous shift of the pedestals of neighbouring channels. The problem arises when the energy of a cluster of 3x3 cells is calculated. A shift of all pedestals by ± 1 adc counts corresponds approximately to ± 300 (150) MeV per cluster in the inner (middle) part of the calorimeter. In case of uncorrelated noise the shift of the

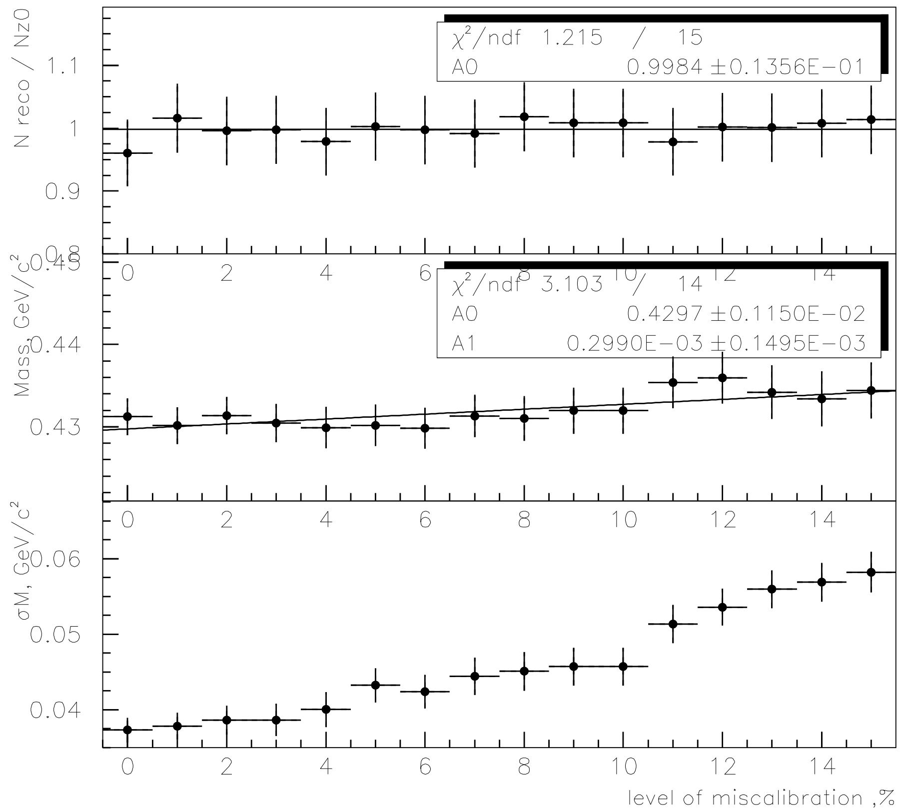

Figure 26: The dependence of the parameters of the reconstructed χ_c signal on the level of the miscalibration (Monte Carlo). The level "0" corresponds to the perfect calibration.

different channels will cancel. During the considered period correlated shifts of up to 10 adc counts were observed. A procedure based on the known correlation between channels was developed to compensate this effect [16]. It was checked with Monte Carlo by shifting all cells from the cluster of the χ_c photon by the same amount. The figures 27 and 28 show the effect of the correlated noise and noise suppression mechanism on the reconstruction of the χ_c signal. When the noise suppression mechanism is not applied the signal is still observed but it is shifted with respect to the nominal position. The amount of events observed with and without suppression mechanism agrees with each other.

The effect of the correlated noise is less problematic for the reconstruction of J/ψ in the electron channel since the energy of the electrons is much higher.

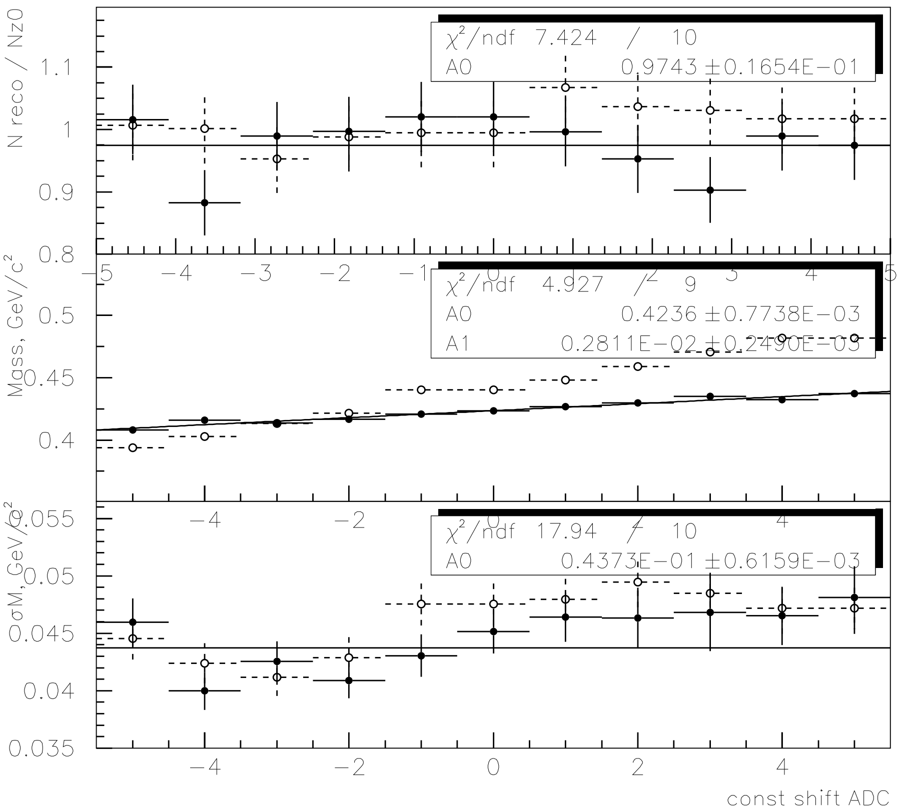

Figure 27: The dependence of the reconstructed χ_c signal on a constant correlated shift of the pedestals in the ECAL (MC). The shift is expressed in adc values. Empty points show the distribution of the events with noise simulated; filled points present the distributions after correction.

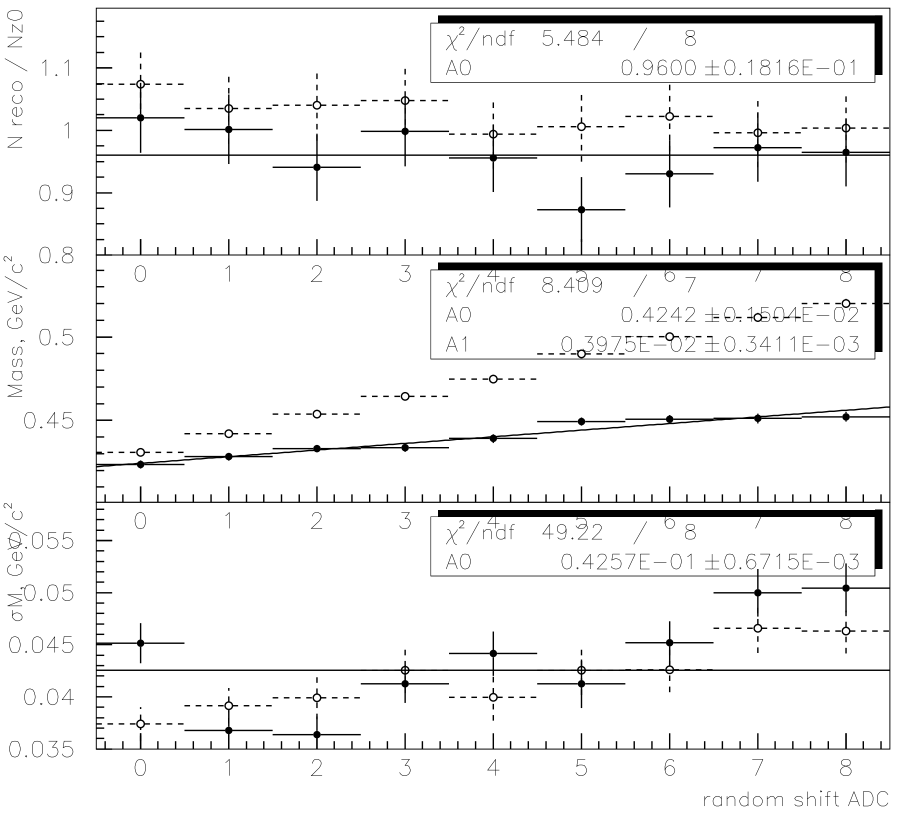

Figure 28: The dependence of the parameters of the reconstructed χ_c signal on the correlated shift of the pedestals in the ECAL (MC). All channels of the cluster are shifted by the same adc value, which itself is distributed according to Poisson statistics with average 0 and fixed width. This width is shown at x axis. Empty points show the distribution of the events with noise simulated; filled points present the distributions after correction.

ECAL dead channel position. To estimate the effect of the variance in the position of the ECAL dead channels the simulation of the ECAL response in different runs was performed. The maps of the dead channels from nine largest runs analysed were used. They were distributed equally over the entire period. The variance in the efficiency estimation for the different runs is smaller than the efficiency uncertainty and the systematic error is neglected.

Fixed width of the distribution. The width of the ΔM distribution is fixed on the basis of the MC spectrum. The systematic uncertainty results from the uncertainties in the calibration precision and the noise level of the ECAL. On base of the fig. 26, 27 and 28 an error of 6% is assigned. The fit of the ΔM distributions with released width confirms the estimations. In this case there is no systematic uncertainty but the statistical error on the N_{χ_c} increases accordingly. The width obtained from this fit is within 1 standard deviation from 45 MeV/c^2 which is used as default.

Variation of cuts. The stability of the results with respect to a variation of the cuts was studied for all subsamples. The dependence of the number of J/ψ and χ_c observed as well as the efficiency of the photon was checked as a function of a cut on one given parameter while keeping constant the values of all other cuts. This check was done for the major cuts on N_{vds}, N_{clus}, E_{clus} and E_{cent}/E_{clus}. The distributions obtained from the μ-C sample are shown on the figures 29, 30,31 and 32, respectively. Each plot contains the estimated ratio R_{χ_c}, the mass position of the signal from the fit of the data sample, and the efficiency of the photon from Monte Carlo entering the determination of R_{χ_c}. The dependence of $N_{J/\psi}$ is shown for the first two distributions, too.

No systematic dependence of the estimated R_{χ_c} on the cuts is found except for the dependence on the energy of the photon. There the contribution of soft clusters ($E_{clus} < 1.5$ GeV) results in a systematic overestimation of the R_{χ_c} because the photon reconstruction efficiency is underestimated. An energy threshold above 4 GeV results in a shift of the maximum of the ΔM distribution into the χ_c region and leads to an underestimation of the value of R_{χ_c} . The threshold used for the final result ($E_{clus} > 3.0$ GeV) lies is in the middle of the region where the distribution is essentially flat.

The total systematic uncertainty is estimated to be 6% from the variance of estimated R_{χ_c} .

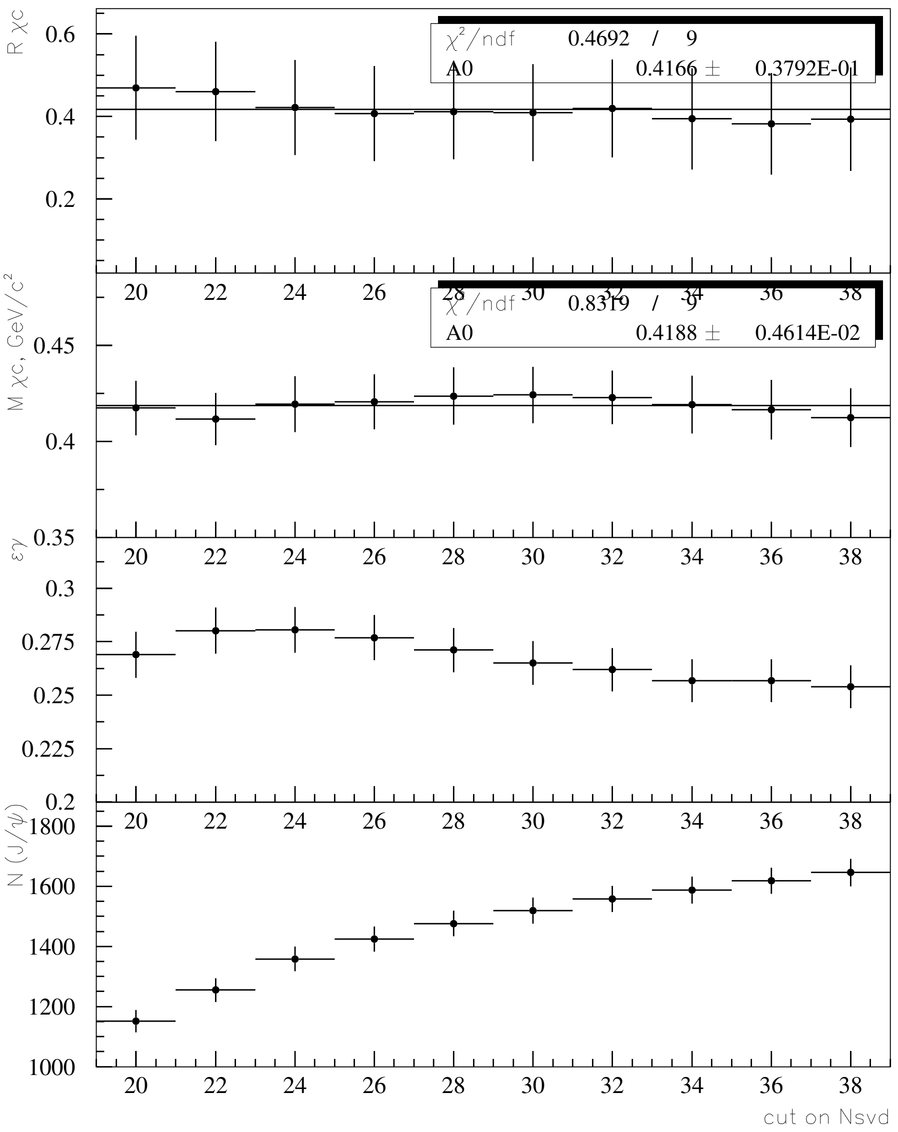

Figure 29: The variation due to the upper limit on the number of reconstructed tracks in the VDS, N_{vds}. The plots from top to the bottom are: ratio of the J/ψ produced via χ_c estimated in the μ-C sample; the mass position of the observed signal; the efficiency of the photon reconstruction with the given set of cuts, and the number of J/ψ passing the cut.

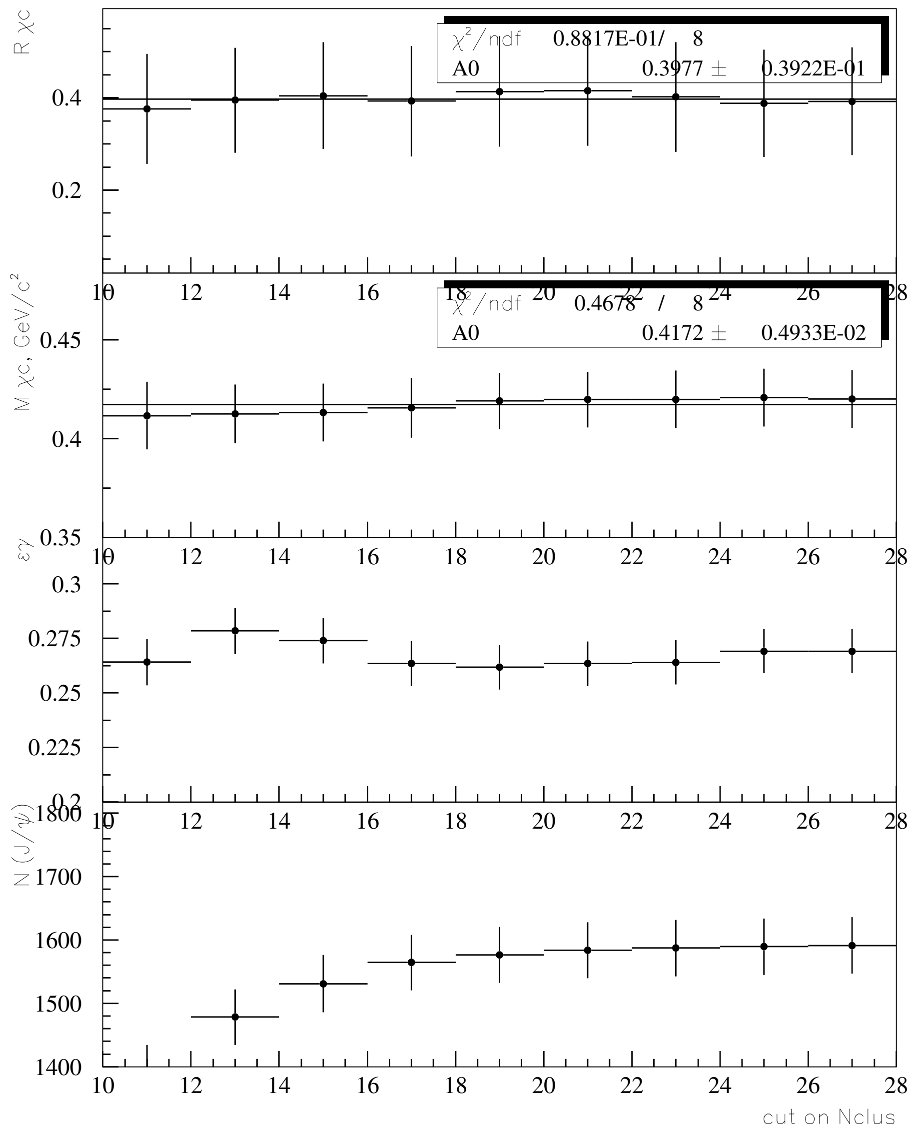

Figure 30: The variation due the upper limit on the number of the energetic ECAL clusters N_{clus}. The plots from top to the bottom are: ratio of the J/ψ produced via χ_c estimated in the μ-C sample; the mass position of the observed signal; the efficiency of the photon reconstruction with the given set of cuts, and the number of J/ψ passing the cut.

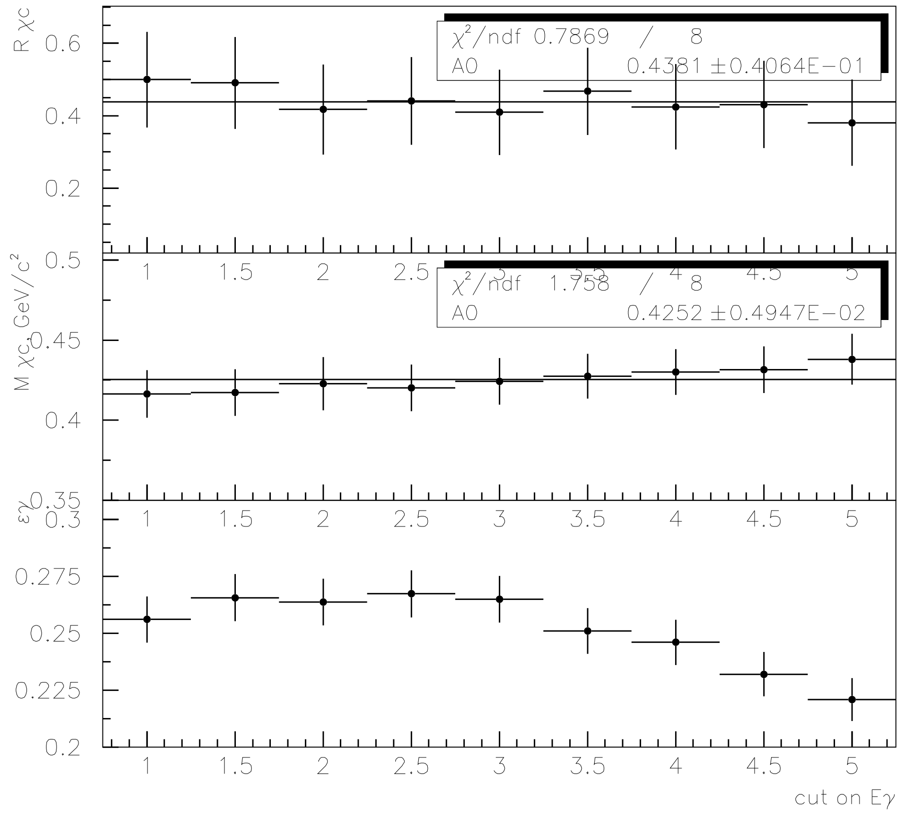

Figure 31: The variation due to the lower limit on the energy of the photon candidate E_{clus}. The plots from top to the bottom are: ratio of the J/ψ produced via χ_c estimated in the μ-C sample; the mass position of the observed signal; the efficiency of the photon reconstruction with the given set of cut.

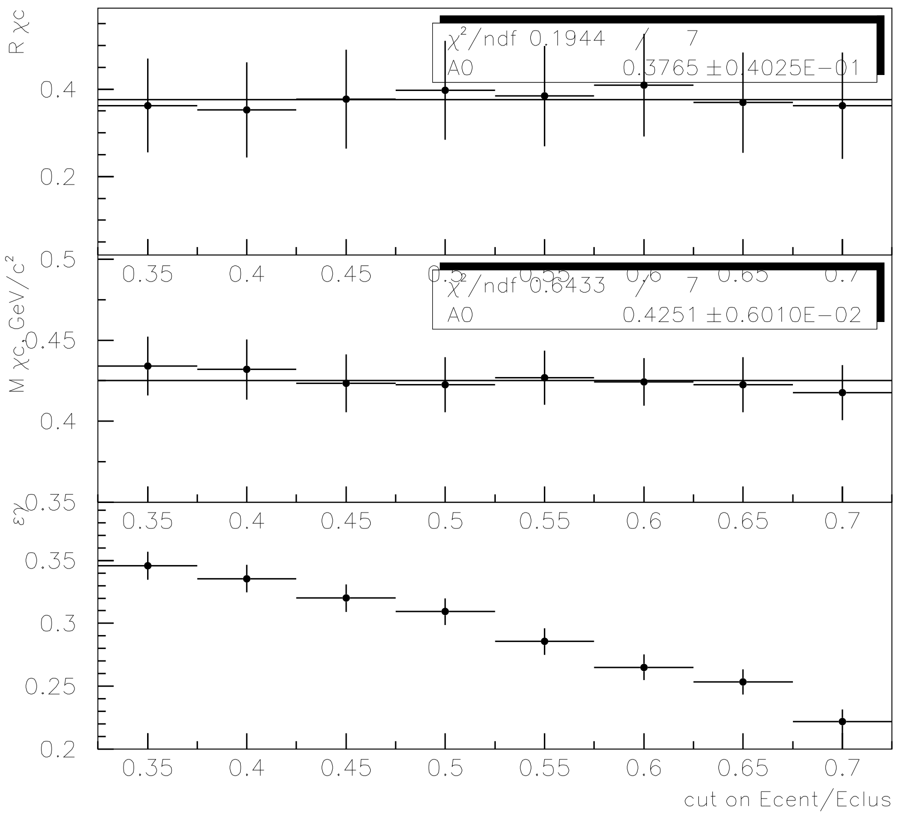

Figure 32: The variation due to the lower limit on the energy of the central cell to the total energy of the cluster E_{centr}/E_{clus}. The plots from top to the bottom: ratio of the J/ψ produced via χ_c estimated on μ-C sample; the mass position of observed signal; the efficiency of the photon reconstruction with the given set of cuts. The very first bin indicates the case the cut is not applied.

Dependence on run period To check that the observed signal is not related to the specific run conditions, the large samples μ-C and e-C were divided on several parts. The χ_c signal is distributed over all parts as seen from fig.33. The reconstructed numbers for χ_c and J/ψ in each part agree with the final estimation of R_{χ_c} .

Binning of histogram. The result of fit procedure is stable with respect to the number of bins in the ΔM plot.

Summary of systematic uncertainties. The main contributions to the relative systematic uncertainty are summarised in the tab.13. The total systematic uncertainty is 10.5%. All sources are the same for different samples.

	Relative Uncertainty
Model dependence	5%
Detector material	2%
Miscalibration	1%
Correlated noise in ECAL	3%
Usage of fixed width	6%
Dependence on cuts	6%
Total Systematic uncertainty	10.5%

Table 13: The relative systematic uncertainties.

Limited MC statistics. The precision of the photon reconstruction efficiency ε_γ is restricted by the MC statistics. As shown in tab.12 the uncertainty is $\sim$ 4% for μ-C and e-C and $\sim$ 8% for μ-Ti and e-Ti. This is much smaller than the statistical error in N_{χ_c} estimation. However, the limited MC statistics affects the estimation of other systematic uncertainties such as the dependence on the production model or effects of noise in the ECAL. To distinguish between such effects one would need a larger MC sample. We solve the problem by assuming all errors (including the error on ε_γ) to be independent. In this way we overestimate the systematic uncertainty.

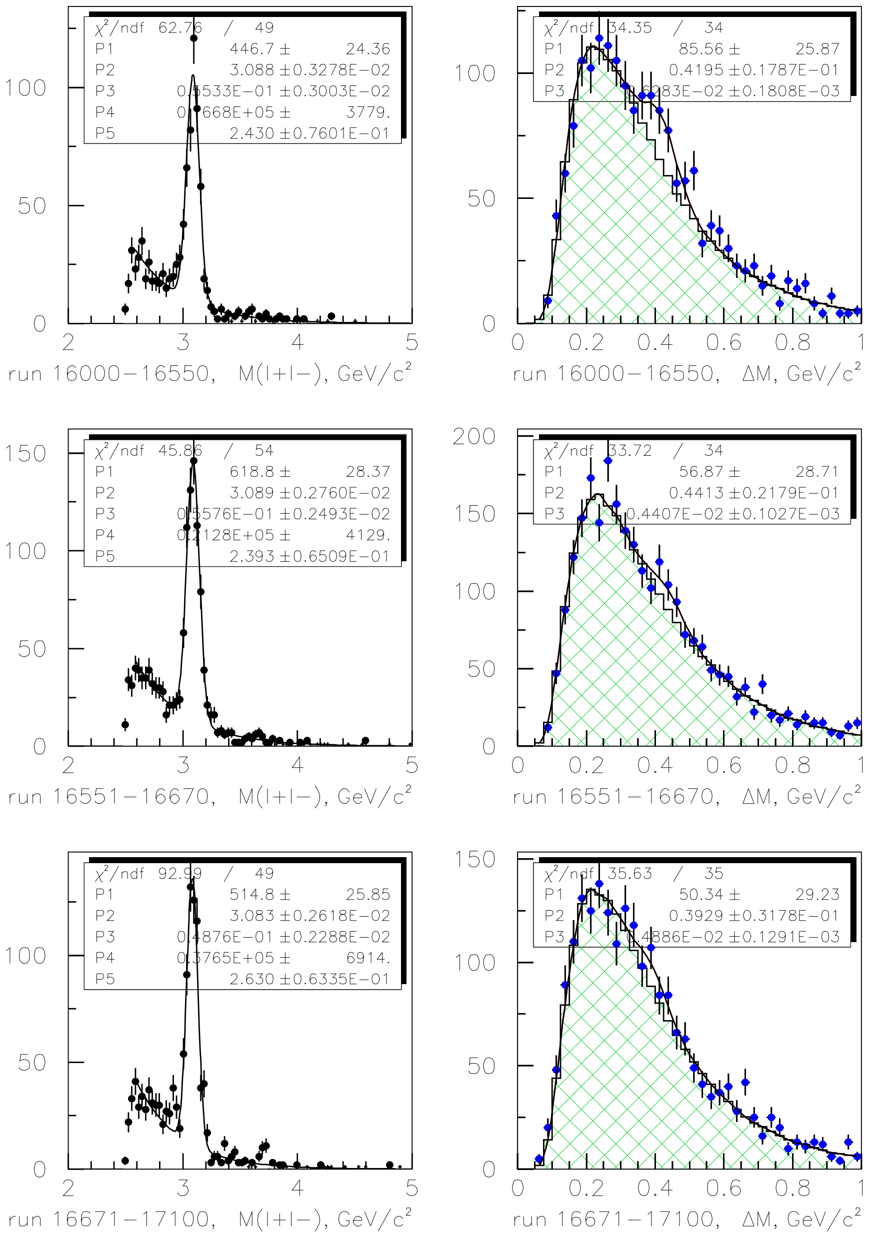

Figure 33: Division of the μ-C sample into three run period as indicated on the bottom of each plot. The left column presents the invariant mass distribution of muon candidates while right column shows the corresponding δM distribution.

11 Estimation of the R_{χ_c} and the comparison of the results with previous measurements.

The results for the ratio R_{χ_c} (see eq.1 and eq. 3) are summarised in table 14. There the number of J/ψ is taken from fig.10 and fig.13 and multiplied with the efficiency of the mass cuts from tab.7 and 9, respectevely. The error on the $N_{J/\psi}$ for e-C and e-Ti includes the additional uncertainty due to the parametrization (see sec.6.3). The N_{χ_c} value is obtained from the fit of the δM spectra (see fig.23). The photon reconstruction efficiency is taken from tab.12 for the NRQCD model.

	μ-C	μ-Ti	e-C	e-Ti
$N_{J/\psi}$	1516 ± 39	647 ± 25	1180 ± 83	382 ± 40
N_{χ_c}	165 ± 47	64 ± 34	121 ± 38	31 ± 27
ε_γ,%	26.5 ± 1.1	27.1 ± 1.8	32.8 ± 1.5	32.7 ± 2.6
R_{χ_c}, %	41 ± 12	37 ± 20	31 ± 10	25 ± 22

Table 14: The result for R_{χ_c}. The error on the R_{χ_c} includes the statistical uncertainties on $N_{J/\psi}$ (also due to the parametrization), N_{χ_c} and ε_γ (due to limited MC statistics). No other uncertainty is included.

All results are in agreement with each other. The weighted average of the μ-C and e-C results is:

$$< R^C_{\chi_c} >= 0.358 \pm 0.055 \pm 0.036 \tag{23}$$

The average of the μ-Ti and e-Ti is:

$$< R^{Ti}_{\chi_c} >= 0.310 \pm 0.104 \pm 0.031 \tag{24}$$

where the first uncertainty is the statistical error (including the one in ε_γ due to limited MC statistics), and the second is the total systematic uncertainty taken from tab.13.

The result is in agreement with all but one previous measurements [7] (see fig.34). Although the statistics collected is not big, the uncertainty on the HERA-B $R^C_{\chi_c} = 0.36 \pm 0.057 \pm 0.036$ measurement is comparable with the measurements of the E705 ($R^{E705}_{\chi_c} = 0.30 \pm 0.04$) and the CDF ($R^{CDF}_{\chi_c} = 0.297 \pm 0.017 \pm 0.057$). The obtained HERA-$B$ values supports the NRQCD model and the CEM, and excludes CSM if nuclear effects are neglected.

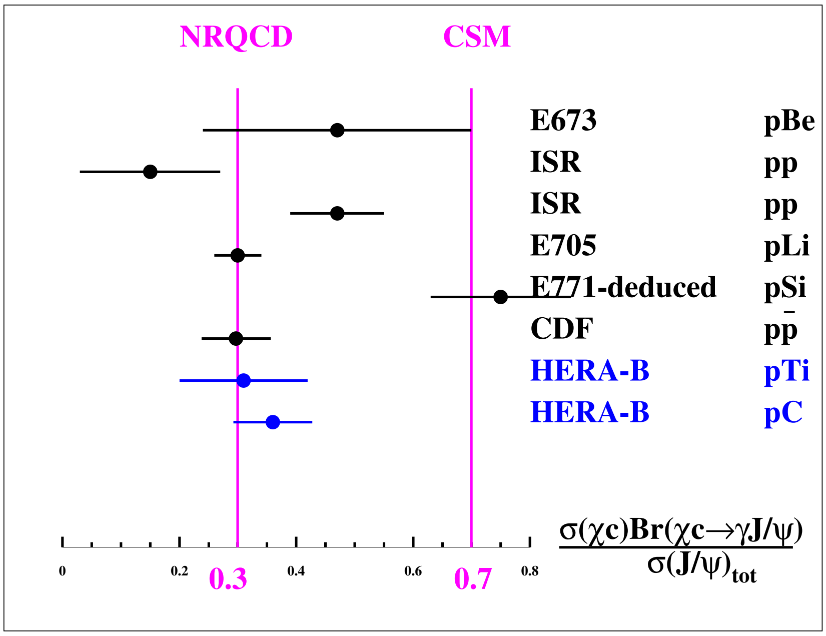

Figure 34: Comparison of R_{χ_c} as measured by HERA-B, with the other experiments. The vertical lines represent the predictions from NRQCD and CSM. The E771 measurement was deduced from the published $\sigma(\chi_{c1})$, $\sigma(\chi_{c2})$ and $\sigma(J/\psi)$. The error shown for this measurement might be underestimated since the correlation between $\sigma(\chi_{c1})$ and $\sigma(\chi_{c2})$ is not discussed [32].

As discussed in sec.1 there are models which predict a nuclear dependence of R_{χ_c} . On the base of these model we calculate the increase of $R^C_{\chi_c}$ to be not more than 5% with respect to the $R^0_{\chi_c}$ of the proton-proton collisions and the increase of $R^{Ti}_{\chi_c}$ to be not more than 8% with respect to $R^0_{\chi_c}$. Unfortunately, the uncertainty of the measurements presented is larger than these values.

In addition, we would like to notice that the present world sample of reconstructed χ_c produced in $p-A$ collisions consists of about 2000 events where the HERA-B contributed about 20%. If about 10^6 or more J/ψ events will be collected during the next run period of 2002 year an outstanding measurement of R_{χ_c} fraction should be possible. The detector upgrade will allow to decrease the systematic uncertainty (e.g. electronic noise in the ECAL). The expected accuracy will allow to distinguish the NRQCD and the CEM models as well as to test nuclear models.

12 Conclusion.

The fraction of J/ψ produced via χ_{c1} and χ_{c2} states is an important observable to distinguish between different models of J/ψ hadro-production and nuclear suppression.

Using the HERA-B di-lepton triggered data of the year 2000 with proton-carbon and proton-titanium interactions the decay channels $\chi_c \to J/\psi\gamma$, $J/\psi \to \mu^+\mu^-, e^+e^-$ are reconstructed. The photon is identified as a cluster in the ECAL with efficiency of about 30%. A clear signal is observed in carbon samples with di-muons ($N_{\chi_c} = 165 \pm 47$) and di-electrons ($N_{\chi_c} = 121 \pm 38$). The statistics with the titanium wire is smaller: $N_{\chi_c} = 64 \pm 34$ and 30 ± 27 in di-muon and di-electron samples, respectively. These data increases the world sample of the observed χ_c produced in $p-A$ collisions by 20%.

The fraction of J/ψ produced via feed down of χ_c is estimated to be $0.36 \pm 0.055 \pm 0.036$ in proton-carbon interactions. The R_{χ_c} for titanium is $0.31 \pm 0.104 \pm 0.031$. The first error is statistic while the second is systematic. The major systematic uncertainties are due to uncertainties in the production model used for simulation, the cluster energy threshold, χ_c mass resolution variation and (in the case of the electron channel only) to the number of J/ψ, $N_{J/\psi}$. The result is independent on the cuts applied.

The HERA-B result is in agreement with the previous measurements. The contribution of the HERA-B to the world knowledge of the relative production rates of charmonium in the $p-A$ collisions is significant. The obtained HERA-B values supports the NRQCD model and the CEM, and excludes the CSM if the nuclear effects are neglected. The nuclear effects are expected to be too small to be checked with the available statistics.

Acknowledgements

The discussions with Th.S.Bauer, A.Christensen, M.Danilov, W.Hulsbergen, F.Ould-Saada, B.A.Petersen, D.Samtleben, F.Sanchez, S.Shuvalov, U.Uwer, M.Villa and A.Zoccoli were especially useful for the analysis. The author has the pleasure to see that the analysis of the χ_c signal in the muon J/ψ data was performed in parallel by A.Christensen. His results can be found in his diploma thesis.

References

[1] C.H.Chang, Nucl.Phys. **B172** (1980) 425; R.Baier, R.Rückl, Phys.Lett. **B102** (1981) 364, Z.Phys. **C19** (1983) 251.

[2] P.Cho, A.Leibovich, Phys.Rev. **D53** (1996) 6203; M.Beneke, I.Z.Rothstein, Phys.Rev. **D54** (1996) 2005.

[3] H.Fritzsch, Phys.Lett. **B67** (1977) 217.

[4] R.Gavai *et al.*, Int.J.Mod.Phys. **A10** (1995) 3043

[5] G.A.Schuler, Eur.Phys.J. **C8** (1999) 273

[6] T.Affolder *et al.*, Phys.Rev.Lett. **85** (2000) 2886

[7] A.G.Clark *et al.*, Nucl.Phys. **B142** (1978) 29; D.A.Bauer *et al.*, Phys.Rev.Lett. **54** (1985) 753; L.Antoniazzi *et al.*, Phys.Rev.Lett. **70** (1993) 383; T.Alexopoulos *et al.*, Phys.Rev. **D62** (2000) 032006; F.Abe *et al.*, Phys.Rev.Lett. **79** (1997) 578

[8] R.Vogt, Phys.Rev. **C61** (2000) 035203

[9] R.Vogt, hep-ph/0107045

[10] HERA-B Collaboration, HERA-B-02-005

[11] HERA-B, DESY-PRC-95-01

[12] O.Igonkina, Ph.D. thesis, to be published.

[13] K.Ehret *et al.*, HERA-B-00-102

[14] F.Sanchez HERA-B-01-120

[15] S.Shuvalov, HERA-B-00-165

[16] M.Villa

[17] T.Sjöstrand, Comp.Phys.Comm. **82** (1994) 74.

[18] H.Pi, Comp.Phys.Comm. 71 (1992) 173

[19] O.Igonkina, HERA-B-01-067

[20] J.Ivarsson *et al.*, HERA-B-99-067

[21] R.Brun *et al.*, Prog.Lib Q123 CERN(1993)

[22] C. Caso et al, Review of Particle Physics, The European Physical Journal, C15 (2000) 1

[23] http://www-hera-b.desy.de//subgroup/software/arte/gean/GEOMETRY.html

[24] O.Igonkina, talk given at J/ψ group meeting 23.04.2001 http://www-hera-b.desy.de/subgroup/physics/herab/jpsi/jpsi_mumu ;

[25] M.Villa, HERA-B-01-093

[26] The plots for the estimation of the efficiency of the bremstrahlung on data are kindly provided by M.Mevius

[27] M.Bruinsma, HERA-B-01-087

[28] I.Matchikhilian *et al.*, Lisbon World Scient. (1999) 411

[29] O.Igonkina *et al.*, HERA-B-00-103

[30] V.Alberico *et al*, Calor97 Proceedings.
http://www-hera-b.desy.de/subgroup/detector/ecal/talks/calor97_villa.ps

[31] http://www-hera-b.desy.de/subgroup/detector/ecal/runlog/welcome.html

[32] T.Alexopoulos *et al.*, Phys.Rev. **D62** (2000) 032006;